



Performance analysis and comparison between bifacial and monofacial solar photovoltaic at various ground albedo conditions

Marzia Alam^{a,*}, Mehreen Saleem Gul^a, Tariq Muneer^b

^a Heriot-Watt University, School of Energy, Geoscience, Infrastructure and Society, Boundary Rd N, EH14 4AS Edinburgh, UK

^b Edinburgh Napier University, School of Engineering and the Built Environment, 10 Colinton Rd, EH10 5DT Edinburgh, UK

ARTICLE INFO

Article history:

Received 23 April 2022

Revised 15 January 2023

Accepted 17 January 2023

Available online 21 January 2023

Keywords:

Bifacial PV

Ground albedo

Rear irradiance gain

Bifacial gain

Specific yield

ABSTRACT

This paper analyses and compares the performance between a bifacial and a monofacial PV system based on the tests conducted at Heriot-Watt University, UK. The module's performance was observed on different ground reflective surfaces: concrete, white tiles, soil, and white pebbles. The rear side irradiance and bifacial energy gains are analysed. The power output is examined for a sunny and cloudy days, and yearly energy mapping is shown. Correlation studies are performed, and empirical model are developed between (i) clearness index and rear irradiance gain; (ii) rear irradiance gain and bifacial energy gain; (iii) total irradiance and power output. Based on the annual rear irradiance gain analysis, the highest gain range is found for white pebbles and white tiles ground surface (>30 % gain) and lowest for soil surface within the 5 %–10 % range and for concrete, >20 %. Regardless of the ground reflective surface, the probability is low that the bifacial energy gain is more than 30 %. Finally, a case study is discussed to perform a sensitivity analysis of a bifacial PV project's Levelized cost of electricity (LCOE). The sensitivity analysis shows that by using an enhanced ground albedo surface, the LCOE of the bifacial PV project can be reduced to 7.15p/kWh. The results show consistency with simulations output ran in PVSyst for different locations across the UK and the reported bifacial gain worldwide.

© 2023 The Author(s). Published by Elsevier Ltd. This is an open access article under the CC BY-NC-ND license (<http://creativecommons.org/licenses/by-nc-nd/4.0/>).

1. Introduction

Bifacial PV is a leading photovoltaic technology that captures sunlight from the module's front and rear sides. It can achieve significant energy gain compared to conventional monofacial PV from its reflected irradiance on the rear side. There has been enormous research in simulation and validation under various test conditions in the last five years. A significant turning point in PV history was the world's lowest bid submitted for a bifacial PV project of 300 MWp by EDF/Masdar, costing 1.79 USct/kWh, which was denied due to negative bankability evolution [1]. However, these bids worried investors and the PV community as they had not yet planned for bifacial PV in their roadmap, and since then, many big companies have started research and development on the practical and theoretical evaluation of bifacial technology [1]. To make the technology viable, the researchers have developed multiple methods to reduce the Levelized cost of electricity (LCOE) [2]. In a gap of 5 years, there has been a significant reduction in LCOE; for example, an 800 MWp solar PV plant is planned to be built in

Qatar at 1.56 USct/kWh [3]. The success of this new technology will depend on field test results and its validation across different parts of the world.

There has been ongoing research on the bifacial PV system for more than one decade. For example, New Energy developed a 30-kW fenced type vertical bifacial system close to the Aichi airport, Japan, in 2006. The energy produced from this research plant met the energy demand of nearby sewage treatment plants and utility centres [4]. A numerical model was developed to predict the power output of the noise barrier built in the Netherland [5]. A simulation model was developed and validated under actual test conditions to determine the optimum bifacial PV installation parameter. It was shown that a vertically installed module could achieve a higher energy yield than the south-facing module [6]. The bifacial module has been studied for building applications, such as its use as a building envelope. Research has shown that electricity generation can be improved by 4.7 %–18.8 % depending on indoor lighting and bifaciality, which can be further increased by enhancing the indoor reflectance of the building ceiling [7]. Bifacial PV modules' performance was observed at snow climate conditions in Sweden at different tilt angles varying from 0° to 90°. During snow coverage from January to March, the lower angle

* Corresponding author.

E-mail addresses: ma410@hw.ac.uk (M. Alam), m.gul@hw.ac.uk (M.S. Gul), T.Muneer@napier.ac.uk (T. Muneer).

module has a minimum energy output compared to others. Overall, for January–May’s observation period, the best energy output was achieved at 35°–45° [8]. At the bifacial photovoltaic test site, Denmark, a 26 kWp bifacial fixed-tilt and single-axis tracking tracking system were compared between measured and simulated data [9]. Based on the global perspective analysis, it is found that at a ground albedo of 0.25 for soil, the bifacial gain is about 10 % which increases by 20 % at an albedo of 0.5 and an installation height of 1m [10]. A comparison between south-facing bifacial and monofacial modules shows that an annual bifacial gain of 21 % can be archived, and the highest performance was achieved during spring [11]. Three years of observation at the France Alps showed degradation of bifacial gain by about 3.6 % for a three kWp system installed at 0.8m height and ground albedo of 40 %. TUV Rhineland installed PV systems in the USA, Germany, Saudi Arabia, and Chennai. Based on the analysis of ground surfaces made of gravel, the gain is around 13.5 %–15 % [12,13]. A simulation tool was developed at the Enel innovation lab at Catania to compare the performance of ground mount and floated PV systems [14]. A comprehensive review has been carried out to present a detailed analysis of bifacial PV’s thermal and electrical performance [15]. A mathematical model was developed to determine a building-integrated PV system’s electrical and thermal energy balance [16]. A miniaturized test array was set up as a commercial bifacial PV system replica in Switzerland [17]. The International Energy Agency Photovoltaic Power System Programme (IEA PVPS) published a report in 2021 on the field performance of BPV from the test carried out worldwide. Participating countries reported are the USA, France, Germany, Sweden, Switzerland, Chile, Canada, Denmark, Italy, and Finland. IEA PVPS is a technology collaboration programme that promotes solar PV research worldwide. The summary of the BPV performance at various test locations is shown in Table 1 below.

From the IEA report, it appears that there has been the use of white materials for testing PV performance in the form of white rocks or white pebbles, which are considered high reflectance surfaces. To justify the use of enhanced albedo ground instead of natural ground made of soil or grass, it is a prerequisite that the BPV performance is investigated comprehensively to ascertain how much additional energy bifacial PV can produce compared to monofacial. Moreover, it is more realistic to present the gain at different albedo with a range of values instead of representing it with a single value. S. Xingshu et al. have explained the geographical dependence of bifacial PV performance and developed several empirical equations that can be used for preliminary assessment of location-specific performance evaluation [10]. Their research provides valuable insights into determining the optimal tilt and height of PV installation. However, in that article, two limitations have been highlighted: the lack of long-term data and the use of

satellite-measured solar data, which is less accurate than the on-site or ground station-measured data. The author has also mentioned that the existing analytical equation does not consider location-dependent parameters such as the clearness index, which might lead to accuracy concerns while assessing the performance of bifacial PV [19]. The information is scarce regarding how the rear irradiance gain varies with ground albedo depending on the clearness index representing the location’s clearness and cloudiness and there is a lack of sufficient data about the ranges of gain achievable at different ground-reflectance surfaces.

It is evident that field data is an essential resource in boosting the implementation of bifacial technology. As it can be seen, there have been various research and field testing at different geographical locations across the globe, such as USA, UAE, Chile. There have not been enough field test results on bifacial PV around the temperate oceanic climate known as cfb climate (Fig. 1). The geographical spread in the deployment of bifacial PV across this region is low (1.5 GW–2 GW) compared to Asia, the USA, and the Middle east. Some of the countries in this zone include Western Europe, South America, Northwest Canada. The overall climate conditions of these countries have cool summer and cool winter. These climates are often cloudy and receive a significant portion of diffused solar irradiance, where bifacial PV can be potentially beneficial. This is because the ground-reflected irradiance component received by PV increase with the higher diffuse irradiance component. For example, the UK receives a significant portion of diffuse irradiance, more than 60 % [20], which is in favour of bifacial PV, but there has not been enough research reported on the field performance of BPV in the country. There are many such countries with great potential for bifacial PV, but the unavailability of enough evidence on bifacial PV performance data is impeding the deployment of this technology. The findings of this paper provide an important indication about the expected outcome from the bifacial PV system installation specially in mid to higher latitude countries which received higher portion of diffused irradiance (>50 %). Furthermore, the methodology presented in the paper can be replicated for any location.

Finally, it is understandable that bifacial PV performance depends on the number of modules. The small row benefits from an open non-shaded region and less ground coverage ratio and overestimates the performance gain than the utility-scale plant. In various literature, often overestimated bifacial energy gain is reported [21]. Therefore, the critical questions among researchers, investors, and policymakers are about what energy gain we should expect from this new technology in reality. Hence, this research can be an important benchmark in scaling up the solar PV system at a large scale, considering the outcome of this work as a reference. Here the bifacial energy gain results obtained from this research has been compared with PV systems of different sizes

Table 1
Bifacial gain reported around the world [18].

Location	Site name	Ground surface	Size	Albedo	Bifacial energy gain [%]
USA	Sandia national lab	White rocks, gravels	—	(0.55–0.6), (0.2–0.25)	6 %–45 %
France	INES	white stone	3 kW _p	0.40	8.9 %
Chile	ATAMOSTEC	desert	1MW _p	—	7 %–14 %
Germany	TUV Rhineland	gravel	—	0.28	11.6 %
USA	TUV Rhineland	dark gravel + sand	—	0.13	8.2 %
Saudi Arabia	TUV Rhineland	sand with gravel	—	0.30	12.7 %
Chennai, India	TUV Rhineland	white stone	—	0.50	22.4 %
USA	NREL	grass	75 kW _p	0.26	8.9 %
Sweden	Rise	snow	33.9 kW _p	0.80	18 %–35 %
Denmark	Riso	grass, gravel, white tarp	6.5 kW _p	0.22, 0.20–0.26	5 %–15 %
Italy	RSE	Concrete, grass	1.95 kW _p	0.6	10.4 %
Finland	TUAS	Bituminous membrane, snow	3 kW _p	0.27, 0.10	5 %

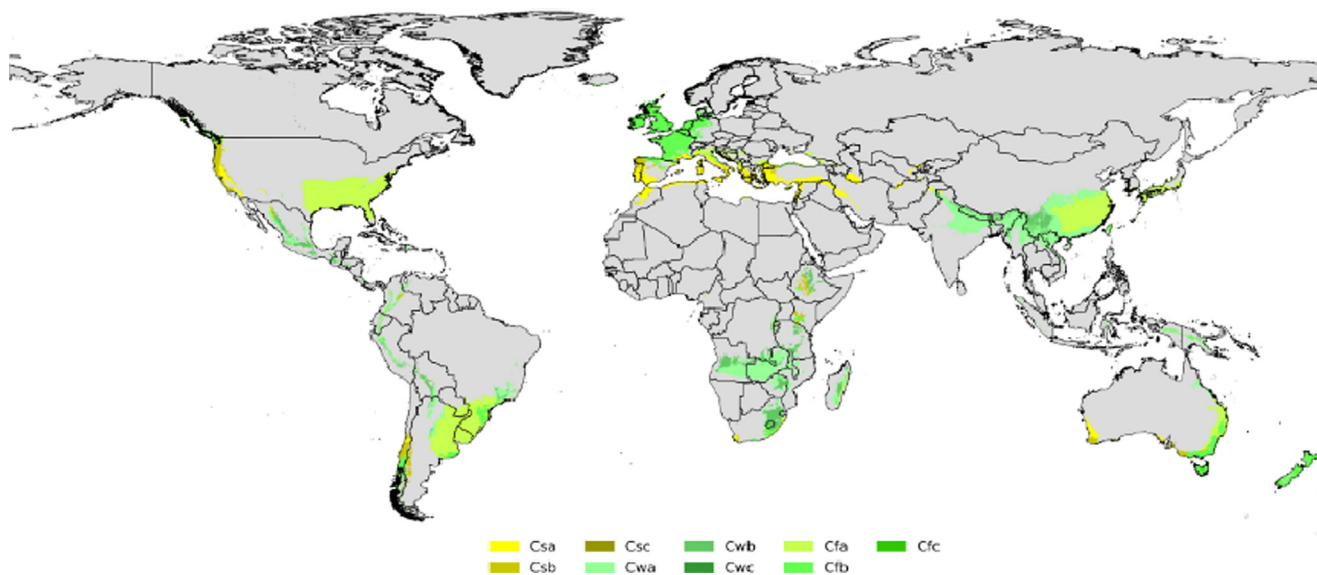


Fig. 1. Countries with temperate climatic conditions [22].

ranging from 43.2 kW to 56.38 MW at different ground albedo conditions in PVSyst. Furthermore, the consistency of the simulated output and the reported bifacial energy gain worldwide has been verified with the data obtained from the test site at the Heriot-Watt, Edinburgh campus.

Multiple variables can affect the performance of bifacial PV, such as module tilt, height, the albedo of the ground surface, mounting structure etc. This paper focused mainly on comparing monofacial and bifacial PV performance at various albedo conditions. The prime objectives of this research are:

- Analysing rear irradiance gain and bifacial energy gain at the various ground surfaces.
- Verify the consistency of the measured field data with simulation study.
- Study of Levelized cost of electricity (LCOE) and its sensitivity analysis for the bifacial project.

2. Methodology

2.1. Experimental setup and design

An off-grid PV system has been built at Heriot-Watt, Edinburgh campus. The experimental setup and system block diagram is presented in Figs. 2 and 4 respectively. The stand-alone PV system consists of two PV modules: one bifacial and one monofacial. Each PV is connected to a 24V battery bank system via a dedicated MPPT charge controller (CC). Each battery is 12V 90Ah and is a sealed lead-acid battery, allowing 80% depth of discharge (DOD). Two loads are connected with the bifacial PV system: a 48Watt portable DC cooler/heater and a resistive load with two 10-ohm resistors in parallel. Monofacial PV is connected with two 20Watt LED lights and one rheostat with a 5A current rating. All the loads are connected parallelly to the battery (instead of the CC load output) via the battery protection unit to avoid overcharge and discharge. All the measured data are passed to two separate data loggers accessible from the computer. One data logger with 32 channels holds the following electrical output: maximum current from PV modules (I_m), the maximum voltage from PV modules (V_m), battery charging current (I_{BAT}), load current (I_{load}) and battery voltage (V_{BAT}). Another data logger stores the meteorological data such as global horizontal irradiance (GHI), global tilted irradiance mea-

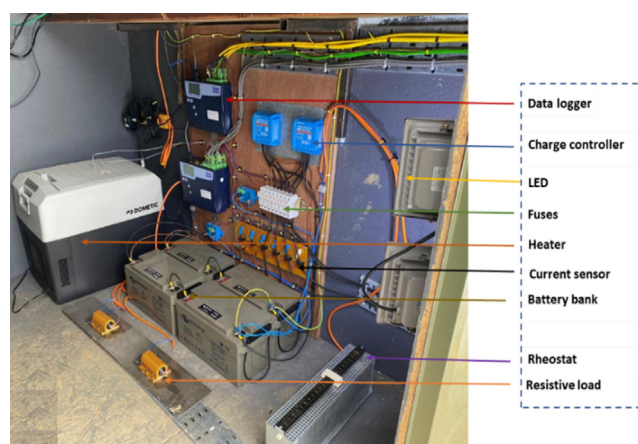


Fig. 2. Experimental setup

sured on the front side (GTI_F), reflected irradiance or global tilted irradiance measured on the rear side (GTI_R) of the module, the temperature measured by thermocouples on the front and backside (T_{front} , T_{rear}) of the module and the ambient temperature (T_{amb}).

Data were collected for 12 months, from June'2021 to May 2022, for the different configurations shown in Table A1. Data were taken in two steps: a short duration consisting of a one-week cycle and a more extended period of three-week. The variables considered are ground albedo, module height and tilt. This paper presents results for concrete, white pebbles and white tiles and soil ground surface (as shown in Fig. 3) at module tilt=45° and heights of 1m and 0.5m. The average albedo for concrete is $\rho = 0.30-0.35$, for white pebbles, $\rho = 0.5-0.6$, for white tiles, $\rho = 0.7-0.8$ and soil surface, $\rho = 0.10-0.15$ respectively. The specification of the modules can be found in the appendix sections (Table A2 and Table A3).

2.2. Data analysis method

Any photovoltaic system performance depends on various conditions for example, daily or monthly weather data variation, such as solar irradiance and temperature. System performance varies depending on the test conditions: PV installation height, ground



Fig. 3. (a) Concrete (b) White tiles, (c) Soil and (d) White pebbles ground surface

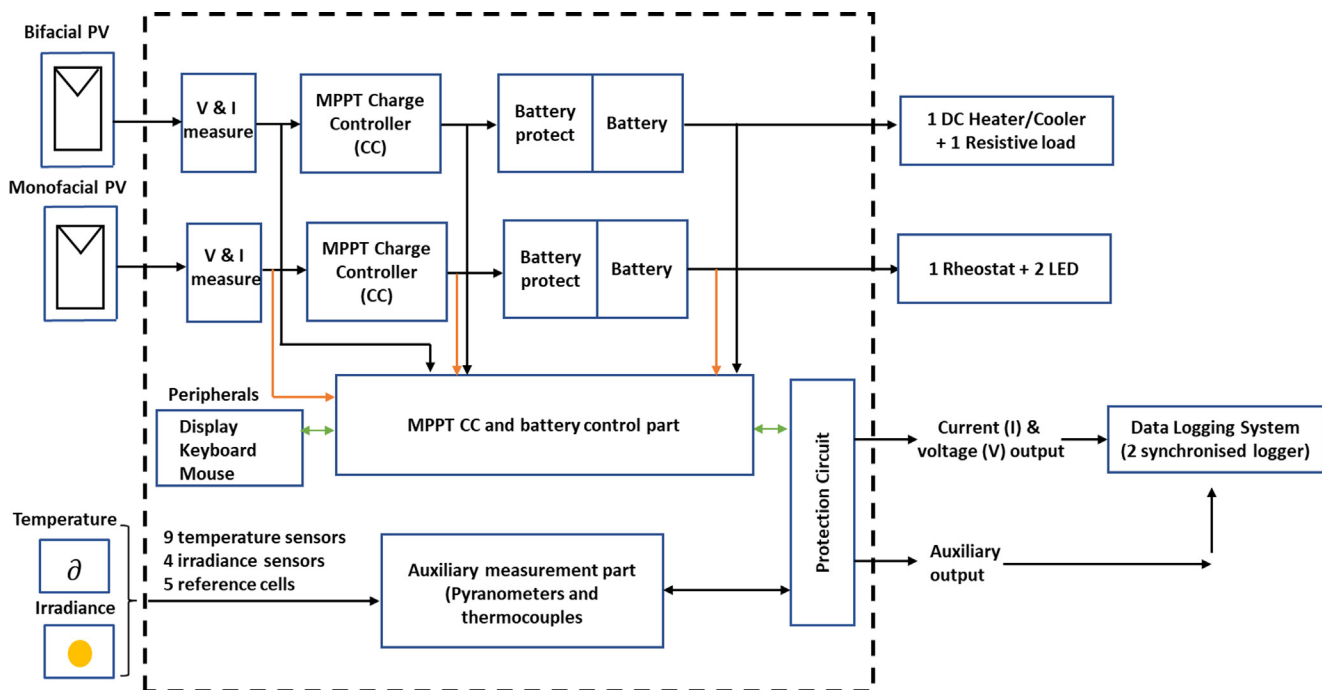


Fig. 4. System block diagram showing bifacial and monofacial PV is connected to the load via MPPT charge controller and battery.

albedo conditions, and module tilt. Monitoring and analysing this complex system are essential to ensure accuracy and minimise measurement uncertainty. The data recording rate is 3s and the system generates about 864,000 data per day. An automatic data analysis module is essential for processing the measured data and converting it into valuable information by statistical analysis, mathematical computation, and graphical presentation. Hence several computation modules have been developed in the Python programming language. The module can be used to run data filtration checks on time series data automatically and compute variable performance metrics such as rear irradiance gain, bifacial energy gain, performance ratio, and specific yield. Some powerful scientific python packages such as Matplotlib, Padas, and NumPy are used to design the module. The data analysis flow diagram is shown in Fig. 5.

3. System performance analysis method

3.1. Calculated and measured variables

(i) **Clearness index, K_T** : One of the important parameters to assess the overall weather condition of any geographical location is to evaluate the clearness or cloudiness of the day. The clearness index is predicted based on the statistical analysis of long-term measurement for 12 months. The daily clearness index (K_T) is calculated by the ratio of daily global horizontal irradiation (GHI [kWh/m²]) and the daily extra-terrestrial irradiation on a horizon-

tal plane (H_0 [kWh/m²]) which is shown in equation (1). The GHI is measured on-site, and H_0 is calculated using equation (2) [23].

$$\text{Daily clearness index, } K_T = \frac{GHI}{H_0} \tag{1}$$

$$H_0 = \frac{24 \times 3600 G_{sc}}{\pi} \left(1 + 0.033 \cos \frac{360n}{365} \right) \times \left(\cos \varnothing \cos \delta \sin \omega_s + \frac{\pi \omega_s}{180} \sin \varnothing \sin \delta \right) \tag{2}$$

Here, ω_s = sunset hour angle, n = days of the year, G_{sc} = solar constant = 1367 w/m², δ = declination angle and \varnothing = latitude of the location.

The low K_T value represents a cloudy sky condition, while the high K_T indicates a clear sky or sunny day. In this research, $K_T < 0.3$ is considered cloudy, and $K_T > 0.6$ is regarded as a sunny day.

(ii) **Albedo or reflectance**: The ground surface albedo is calculated as the ratio of horizontal reflected irradiance (HRI) and the global horizontal irradiance (GHI), can be written as [24]:

$$\text{Albedo}(\rho) = \frac{HRI}{GHI} \tag{3}$$

Three important parameters are used as benchmark criteria to evaluate bifacial PV's performance: specific yield, rear irradiance gain, and bifacial energy gain.

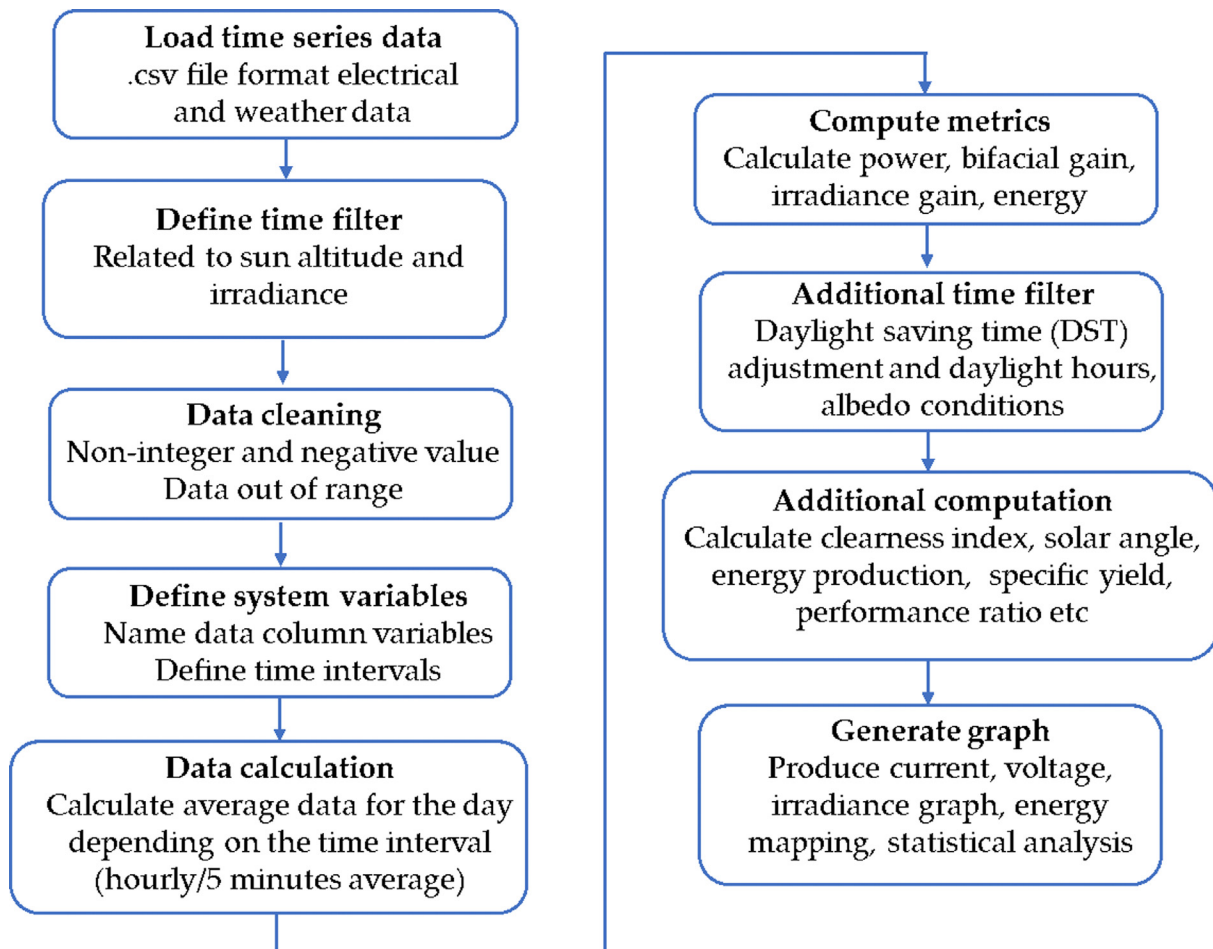


Fig. 5. Data analysis module workflow diagram showing the steps used to calculate various performance matrices of bifacial and monofacial PV.

(iii) Gain measurement

Bifacial PV gain can vary at the module and system levels. It can be defined as follows [18]:

- i. Rear irradiance gain
- ii. Bifacial energy gain

Rear irradiance gain is defined by the ratio of rear and front side irradiance. However, the bifacial PV modules' rear side is not as efficient as the front side. At the module level, the bifaciality factor limits the gain such as:

$$R_G = \frac{GTI - \text{Rear} \cdot b_f}{GTI - \text{Front}} \quad (4)$$

The bifaciality factor, b_f addresses the relative performance of the bifacial PV's rear side to its front side. As per the datasheet, the bifaciality factor is 65 % to 75 %, which is the standard value for a typical n-type module. The bifaciality factor depends on temperature and irradiance level. The rear and front side irradiance is not a constant value, and it varies throughout the day with a solar angle, as shown in the result section.

When comparing two PV systems, the bifacial energy gain or bifacial gain can be computed from the energy output measurement from the two modules separately, provided that identical modules are used. On the system level, the bifacial gain is defined as:

$$B_G = \frac{E_{bi} - E_{mo}}{E_{mo}} \quad (5)$$

Here, E_{bi} and E_{mo} are the energy produced from bifacial and monofacial PV, respectively. The system considers thermal losses, shading loss, cabling loss, inverter loss, mismatch loss and loss due to reduced efficiency at low irradiance.

(iv) Electrical output measurement

The electrical output from a PV system includes current, voltage, power, and energy. The voltage and current are logged using the data logger, and then power is calculated on an hourly basis using equation (6). The calculated power is then aggregated to get the total energy production of the day.

$$P_m = V_m I_m \quad (6)$$

$$E = \sum P_m t \quad (7)$$

V_m and I_m represent current and voltage and P_m is the calculated power, t represents time, and E is the energy generated over time t .

Specific yield refers to the amount of energy (kWh) produced for every kWp (maximum power output at STC) of the module over a certain period. It can be defined as,

$$\text{Specific yield} = \frac{\text{Energy(kWh)}}{\text{Power(kWp)}} \quad (8)$$

The specific yield of a plant depends on location, weather data, amount of irradiance falling on the PV, performance of the module, including sensitivity at different temperature conditions and module orientation. This is also denoted as normalised energy.

3.2. Statistical analysis method

Statistical analyses are helpful to characterise the statistical feature of the data for better understanding and evaluation [25]. The statistical approaches used in this paper is summarised in Table 2 below.

3.3. Uncertainty consideration

Any measurement leads to differences between the measured and actual value, which causes measurement uncertainty. Therefore, it is essential to address the uncertainty before making a statement on the measured value. Uncertainty is the interval within which the measured value is expected to fall at a certain level of confidence. Uncertainty during measurement has been taken into account as per the ISO guideline of uncertainty measurement at a 95 % confidence level and a coverage factor of $K=2$ [28]. The main source of uncertainties are:

- The uncertainty associated with the data logging unit (U_{LOG}).
- The standard uncertainty of the pyranometer U_{py} .
- Uncertainty due to the non-linearity of pyranometers, $U_{nlin-py}$.
- Uncertainty of measurement sensors: thermocouple U_T , current transducer U_C etc.

The combined uncertainty is calculated by taking the square root of the sum of the square of the individual uncertainty as:

$$\text{Uncertainty, } U_{total} = K \times \sqrt{\left(\frac{U_{LOG}}{\sqrt{3}}\right)^2 + \left(\frac{U_{py}}{\sqrt{3}}\right)^2 + \left(\frac{U_{nlin-py}}{\sqrt{3}}\right)^2 + \left(\frac{U_T}{\sqrt{3}}\right)^2 + \left(\frac{U_C}{\sqrt{3}}\right)^2} \quad (18)$$

Let's understand the logger uncertainty first. The logger uncertainty depends on the reading and range accuracy. The accuracy of the logger in the 1.8V range is 0.05 % for reading and 0.025 % for its ranges. For example, an irradiance value of 566 W/m² measured by a pyranometer has an equivalent voltage of 0.35V, estimated at 1.8V ranges. Using equation (19), the calculated uncertainty value is 0.18 %.

$$U_{LOG} = \frac{(U_{reading} \times V_{measured}) + (U_{range} \times V_{range})}{V_{measured}} \quad (19)$$

One of the main uncertainty sources is the pyranometer in irradiance measurement. U_{nlin-p} is associated with the non-linearity of the pyranometer. The manufacture specified linearity is 1.5 %. The value is assumed to remain the same for the entire range of observation. The total uncertainty is the combined effect of the standard uncertainty of the pyranometer (3 %), its non-stability (1 %), non-linearity(1.5 %), and spectral and temperature sensitivity (2 %). The uncertainty due to the non-linearity of the current sensor and its sensitivity error (0.85 %) is 1.35 %, and thermocouple uncertainty is 2.1 % [29]. The total calculated uncertainty at 95 % confidence level is about 6.6 %.

4. Results and analysis

The field data monitoring outcome is discussed in the following order:

- First, solar resource assessment is conducted by comparing measured irradiance and temperature data from a different source.
- Next, a clear sky day and a cloudy day are taken as a reference to analyse the rear irradiance gain and bifacial energy gain for various ground surfaces. Here the term cloudy day indicates both partly cloudy and mostly cloudy days. Instead of using the albedo value of the respective surfaces to represent the different ground, it is addressed by surface types such as white tiles, white pebbles, concrete and soil.

Table 2
Statistical analysis methods used in the article.

Parameters	Mathematical presentation
Mean	Arithmetic average of sets of sample size N and each sample x_j can be represented as: $\mu \text{ or } \bar{x} = \frac{1}{N} \sum_{j=1}^N x_j$ (9)
Median	The middle value of the sampled data sets such that half the numbers will be below and another half above the median value. The mean value is sometimes impacted by extreme observation, such as a very high value of irradiance gain at very low irradiance. In such a case, the median is a more robust marker to represent the data distribution.
Standard deviation	It indicates the distribution of dataset relatives to the mean value. The more fluctuating the datasets are, the higher the standard deviation is observed. The standard deviation for N sets of data can be calculated as follows: $\sigma = \sqrt{\frac{\sum_{j=1}^N (x_j - \bar{x})^2}{N}}$ (10)
Pearson coefficient	An essential quantitative measure which identifies a correlation between variables. It helps to standardise the measured variable by their standard deviation. For two variables x and z, Pearson coefficient, $r = \frac{COV(xz)}{S_{2x} S_{2z}}$ (11) COV(xz) is the covariance of x and z, which indicates the linearity strength between x and z. The absolute value of r is less than or equal to 1; $r=1$ indicates all values are on a straight line which is very unlikely. The range of r helps to demonstrate the strength of the relationship such that $0.9 \leq r \leq 1$ shows a strong linear relationship. $0.7 \leq r \leq 0.9$ indicates a moderate relationship, and $r < 0.7$ shows a weaker correlation.
Mean bias error	Mean bias error is the average deviation of the estimated value from its measured value. For N number of measurements, if the measured or true value is y_j and the estimated value is \hat{y}_j , MBE can be calculated as: $MBE = \frac{\sum_{j=1}^N (y_j - \hat{y}_j)}{N}$ (12)
Root mean square error	RMSE is used to measure the magnitude of absolute error. It can be presented as: $RMSE = \sqrt{\frac{\sum_{j=1}^N (y_j - \hat{y}_j)^2}{N}}$ (13)
P-value	The p-value determines the significance of a model by testing it against the null hypothesis. The null hypothesis indicates there is no correlation between variables ($r=0$), whereas the alternative null hypothesis means there is a relationship between variables. If the p-value is less than or equal significance level, then the null hypothesis can be rejected, and it is concluded that the relationship between variables is statistically significant. The significance level of 95 % (p-value ≤ 0.05) is a standard practice to justify a model. Alternatively, it can be said that the sample data can strongly support the relationship between variables under study at a 95 % confidence interval [26].
Coefficient of determinant, R^2 and predicted R^2	It is essential to evaluate how well the regression model fits the data. The model should be able to explain the dependent variable to some extent. There is various goodness of fit statistics to analyse the regression model, and the coefficient of determinant termed R^2 is one of those. R^2 describe the variation of the dependent variable, which the model can explain. By taking the square of Pearson coefficient r, the R^2 value can be determined. If the model predicted value is \hat{y}_j , the calculated value (or true value) is y_j and the mean value is \bar{y} , the R^2 represents the ratio of variation explained by the model to the total variation such that: $R^2 = 1 - \frac{\sum_{j=1}^N (y_j - \hat{y}_j)^2}{\sum_{j=1}^N (y_j - \bar{y})^2}$ (14)
Statistical distribution	Frequency distribution presents the number of occurrences of an event within a particular bin. It identifies the trends in the sampled data and helps to get insight into the sampled datasets. The cumulative distribution function (CDF) represents the area under the curve ranging from the lowest to the current value of the variable. Normal distribution: The normal distribution, also known as the Gaussian distribution, is a continuous probability distribution around the mean value (μ) of the variables. It can be written as [27]: $A = \frac{1}{\sigma\sqrt{2\pi}} e^{-\frac{1}{2}(\frac{z-\mu}{\sigma})^2}$ (15)
Regression analysis	Regression is a method to fit a linear or non-linear model between the dependent and independent variables. Let's consider a simple linear regression model, $y = mx + c$. The parameter 'm' denotes the slope of the straight line, and 'c' is the intercept that is 'y' value at $x=0$. 'm' and 'c' can be calculated using the following equation: $m = \frac{\sum_{j=1}^N (x_j - \bar{x})(y_j - \bar{y})}{\sum_{j=1}^N (x_j - \bar{x})^2}$ (16) $c = \bar{y} - m \cdot \bar{x}$ (17) and \bar{y} are the mean of x and y, respectively, and N is the total number of observations.

- A correlation study is performed, and empirical models are developed between (i) clearness index, rear irradiance gain, (ii) rear irradiance gain and bifacial energy gain, and (iii) total effective irradiance and power output.
- Then annual energy yield performance is shown for the entire 12-month period (2021–2022).
- After that, PVSyst simulation results are shown to compare the bifacial energy gain results with the field data presented in the paper.
- Finally, a case study is discussed on Levelized cost of electricity (LCOE) for bifacial PV projects.

4.1. Analysis of solar resource data

The reliability of solar energy yield data dominantly depends on the accuracy of the measured solar resources. The solar resource for any given location includes the temperature data, global horizontal irradiance and global tilted irradiance, and for bifacial, the new addition is the global tilted irradiance at the rear side of the PV plane. The parameters measured are discussed below.

(i) **Global horizontal irradiance (GHI)** is the amount of solar irradiance received per unit area of a horizontal surface. It includes diffuse horizontal irradiance (DHI), direct normal irradiance (DNI), and ground reflected irradiance (G_R). GHI can be calculated as [30]:

$$GHI = DHI + DNI \cdot \cos(\theta_z) + G_R$$

Here DHI represents irradiance coming from all directions of the sky per unit area of a surface. DNI is the total irradiance per unit area of a surface that directly comes from the sun. θ_z is solar zenith angle. G_R is the irradiance reflected in the atmosphere after hitting the earth.

(ii) **Global tilted irradiance on the front side, G_{TF}** : solar radiation falls on the module's plane of array (POA).

(iii) **Global tilted irradiance on the rear side, G_{TR}** : the irradiance receives by the rear side of the bifacial PV.

(iv) **Total effective irradiance, G_T** : the contribution from both front and rear irradiance. It is calculated as:

$$G_T = G_{TF} + G_{TR} \cdot b_f \tag{20}$$

The term 'irradiance' means the power density of solar radiation, which arrives per unit area of a surface per unit of time and is typically measured by taking the hourly average. The unit of irradiance is W/m^2 . Often the term 'irradiation' will be used in this paper which is incident energy (sum of irradiance) per unit area taken over a time period, typically hourly, daily, monthly or yearly. The unit of irradiation is Wh/m^2 or kWh/m^2 . If both are given on an hourly basis, then they are equivalent. For example, power density of solar radiation $100W/m^2$ is same as energy produced $100W/m^2$

per hour. The measured data are compared with two historical solar irradiance data sources. These are Meteonorm version 8.0 and Solargis Prospect 2.5. Meteonorm is a global climate database which is obtained from PVSyst. Meteonorm weather data has a temporal resolution of 10–20 years (2004–2013) and a spatial resolution of about 3 km. These datasets are interpolations of satellite images and ground-based measurement data. The Solargis Prospect data are supplied by Wood Group Ltd, UK. These are highly accurate data with a temporal resolution of 25 years (1994–2018) and a spatial resolution of 0.3 km. Fig. 6 compares on-site measured data, Meteonorm and Solargis Prospect data. The total GHI measured on-site from June 2021 to May 2022 is 829.1 kWh/m². However, the on-site measured data is slightly lower, about 3 % with Meteonorm and 7 % with Solargis data (Fig. 6a). This can be due to the presence of nearby buildings on the eastern side of the test site, which causes a few missing early morning data. The annual total global tilted irradiation (G_{Tf}) measured on the front side is 1019.65 kWh/m², which is about 22 % higher than the GHI.

The measured temperature data are compared with the PVSyst, and Solargis Prospect data shown in Figure 6b. The temperature data is about 1°–3.7°C higher than Solargis and Meteonorm data. One reason for this can be the measurement accuracy of ±2.2°C for K-type thermocouples [29] which may cause a slightly higher temperature reading than the actual value. The measured irradiance and temperature data are consistent with the data from various sources. Overall, the measured data showed a good agreement with the Solargis and Meteonorm data. Therefore, results obtained based on the measured data can be considered reliable.

4.2. Rear irradiance gain analysis

The bifacial PV receives a significant portion of rear-side irradiance from the reflected irradiance. The nature of reflected irradiance depends on the direction of the incident light and the hemispherical distribution of diffuse irradiance. Furthermore, it strongly relies on surface properties such as reflectance or albedo of the ground surface. The albedo varies significantly between sunny and cloudy days by 3 %–10 %. White tiles have the highest albedo. It is important to understand the influence of different ground surfaces on the rear irradiance gain of PV. The rear side irradiance gain denoted by R_G of bifacial PV is simply the optical gain of the module. It is expressed as the ratio of global tilted irradiance at the rear side and the global tilted irradiance at its front side. The rear irradiance gain is tested for four ground surfaces:

soil, concrete, white pebbles, and white tiles. Depending on the reflectance of the ground surface, the rear irradiance gain achieved by the bifacial module changes. This is because the higher albedo of the ground causes the reflective irradiance received by the rear side of the module to increase. However, at the module level, the irradiance gain will be limited by the module's bifaciality factor, b_f . As per the data sheet of bifacial PV, a value of 70 % is considered in this paper, and the rear irradiance gain is calculated using equation (4).

4.2.1. Correlation between clearness index and rear irradiance gain

The overall clearness index of the day has an impact on the rear irradiance gain. Hence the daily clearness index (K_T) was calculated for the whole year. The frequency distribution of K_T helps to establish the correlation between the clearness index and rear irradiance gain achieved by bifacial PV. As shown in Fig. 7a, the range of K_T value 0.27–0.37 occurred for the highest number of times during the 351 days observation period. This can be further observed in the cumulative frequency distribution (CDF) plot of K_T in Fig. 7b. The vertical scale in the CDF plot provides the probability. The distribution depicts the probability that K_T lies within the range of 0.38–0.56 is 40 %. The likelihood is minimum (about 7 %) that the K_T value to be greater than 0.60. The CDF indicates the K_T is relatively spread over the range of 0.06–0.69, revealing a fluctuating distribution of the clearness index.

In this research, based on the measured field data, various empirical models are developed using ordinary least square regression (OLS) analysis. OLS fits a line to the data that minimises the error between actual and predicted values. Each model is tested against the R^2 value, root means square error (RMSE) and mean biased error (MBE). The significance of these correlation studies can be further verified by the p-value, which provides a measure of confidence in the proposed model. An important metric is R^2 , which is often dependent on the number of datasets. Any empirical model might show overfit. This can be avoided by the residual plot check and calculating the R^2 predicted value. The accuracy of all models' validity is checked against the R^2 predicted value, which helps to address the quality of the model and its predictions.

The correlation between R_G and K_T for all four-ground surfaces is observed, and regression models are developed, as shown in Fig. 8. The model coefficient values m and c are the empirical coefficients which are site-dependent parameters affected by the reflectance of the ground surface and overall cloud cover. The R^2 value for all four surfaces is found to be low to moderately high.

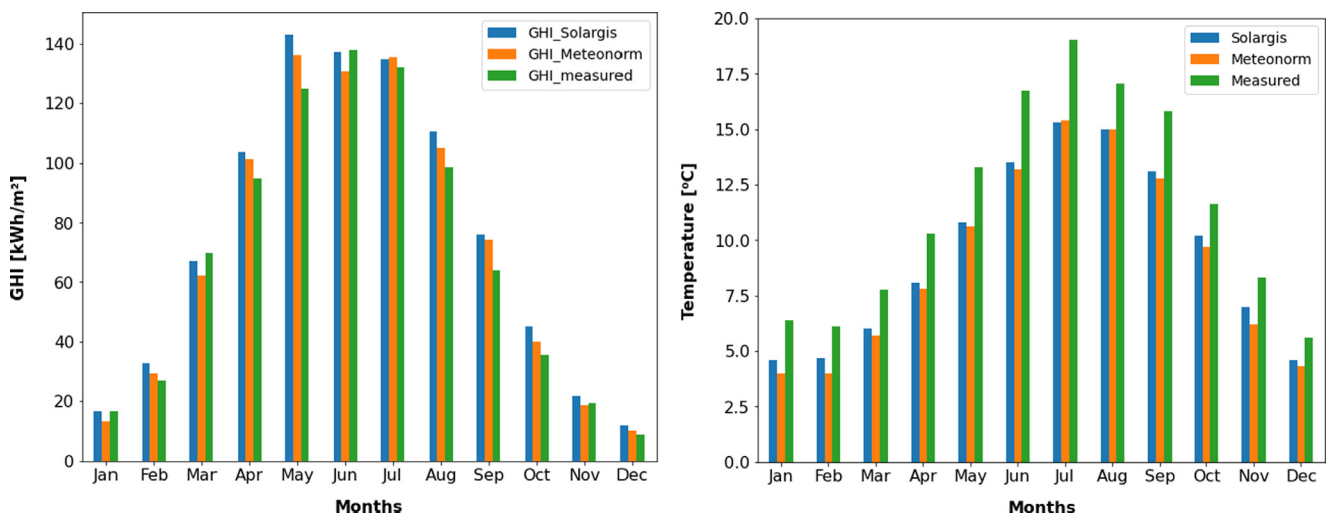


Fig. 6. (a) Annual global horizontal irradiation data measured on-site; (b) annual temperature data for June 2021 to May 2022.

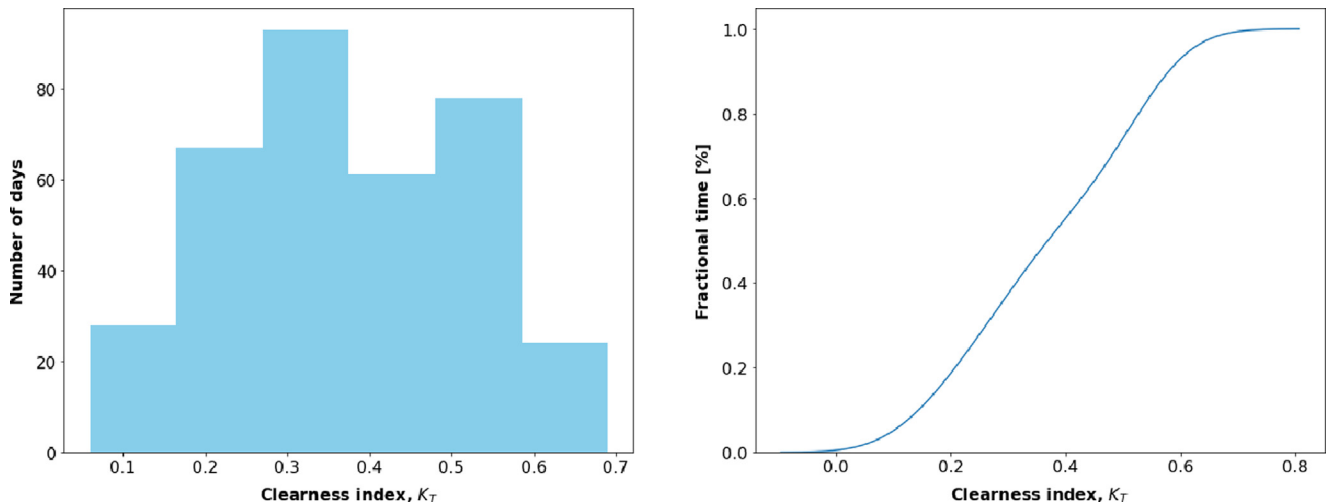


Fig. 7. (a) Frequency plot of clearness index, K_T (left); (b) Cumulative distribution of K_T (right).

This is understandable because only the clearness index cannot fully describe the rear irradiance gain, as the rear irradiance gain also depends on other factors such as module installation height, tilt, installation location and type of ground surface. In all the modelled equations, the negative slope depicts a negative correlation which implies the gain increase on a day with a low clearness index, such as a high gain on a cloudier day than on a sunny day. Therefore, countries with dominant diffuse irradiance will benefit from the deployment of bifacial PV even with low to moderate irradiance conditions. The validity of all models is checked against the R^2 predicted (R^2_{Pred}) value, which is nearly the same as R^2 . The p-value has further verified the significance of these correlation studies. The p-value < 0.05 depicts that the analysis is highly significant for concrete, white pebbles, and white tiles except for soil (p-value > 0.05). The regression analysis led to the development of four empirical equations showing the relationship between R_G and K_T at each ground surface. The equations are tested by checking root mean square error (RMSE) and mean bias error (MBE) to find the average error and bias of the model. The summary of the regression plot is shown in Table 3. Overall, the RMSE ranges between 1%–4%, and MBE is almost negligible.

As shown in Table 3, for the soil ground surface, the low value of $r = -0.3$ indicates a weak correlation between K_T and R_G . The R^2 value can further confirm this. $R^2 = 9\%$ suggests that the irradiance gain for the soil surface has a weak dependency on the clearness index, which is further confirmed with a p-value of 0.23, which is greater than the 95% significance level (p-value ≤ 0.05). The variation in rear irradiance gain at different clearness indexes is closely dependent upon the type of ground surface used. The albedo of the soil surface depends more on its moisture content and surface roughness rather than the overall clearness index of the day. The reflectance of smooth and dry soil surfaces is greater than wet and rough surfaces [31]. The reflectance of the soil can be affected by daily precipitation of the location due to increased moisture content [32] which causes reflectance to decrease. Therefore, the relation between K_T and the rear irradiance gain is not very significant. During data analysis, it was found that for soil surface, the rear irradiance gains on a day with high clearness index did not have much variation as on a day with a low clearness index. For example, 1st July and 5th July 2021. The K_T on these days were 0.65 and 0.21, respectively, and the rear irradiance gain was close to 9% on both days.

The rear irradiance gains for concrete surfaces show moderately low dependency on K_T . The Pearson coefficient value r is -0.55 . The R^2 value depicts that K_T can explain 30% of the variation in R_G . The

correlation coefficient for the concrete is lower than the coefficient for the white pebbles (-0.86) and white tiles data (-0.81), which indicates that the reflectance of concrete has a lower dependency on K_T compared to white pebbles and white tiles. The other parameters that affect the reflectance of concrete are discoloration and mould build-up on concrete. Furthermore, concrete constituent also changes their reflectance. A close relationship is found between R_G and K_T for white pebbles and white tiles surface. White pebbles showed the highest dependency on the clearness index among all four-ground surfaces. The R^2 for the linear regression between K_T and R_G is 75% for white pebbles, which means about 75% variation in R_G can be explained by K_T . The R^2 value for regression between the clearness index and white tiles surface is 65%. The reflectance of white tiles also depends on the incident angle of solar irradiance.

4.2.2. Rear irradiances gain analysis for short duration cycle

In this section, rear irradiance gains analysis is conducted for a sunny and cloudy day. The sunny and cloudy dates are the 8th and 9th of March for concrete, the 24th and 22nd of July for white tiles, the 18th and 15th of March for white pebbles, and the 1st and 3rd July for soil, respectively. Table 4 summarises the average rear irradiance gain on a sunny and a cloudy day in terms of three different statistical criteria: mean, median and standard deviation. The mean gain for the concrete surface on a mostly sunny day was about 10.38% in March for a clearness index $K_T = 0.62$.

The highest gain for pebbles' surface on a sunny day was 11.39%. There was a sharp rise in the gain for white tiles surface for two more obvious reasons: White tiles are an example of a very smooth and shiny surface, known as a specular surface. The white tiles' transparent and mirror nature cause specular reflection. Soil surface has the lowest irradiance gain of about 8.79%. The standard deviation of rear irradiance gain from its mean value is lowest with white pebbles surface (2.79%) and slightly more with concrete (3.48%) surface. Low standard deviation indicates that most observed data clustered around the average rear irradiance gain value. For soil surface, the S_D is more than white pebbles and concrete by about 1.5%. The standard deviation of rear irradiance gain obtained with white tiles is the highest on a sunny day at about 8.33%. The gain increased for all three reflective surfaces on a cloudy day due to more diffused light at the rear side. The standard deviation is also low compared to sunny days. Soil's surface has the lowest S_D of 1.11%. Overall, for the high albedo surfaces (concrete, white pebbles and white tiles), the gain is 5%–10% higher on a cloudy day compared to a sunny day.

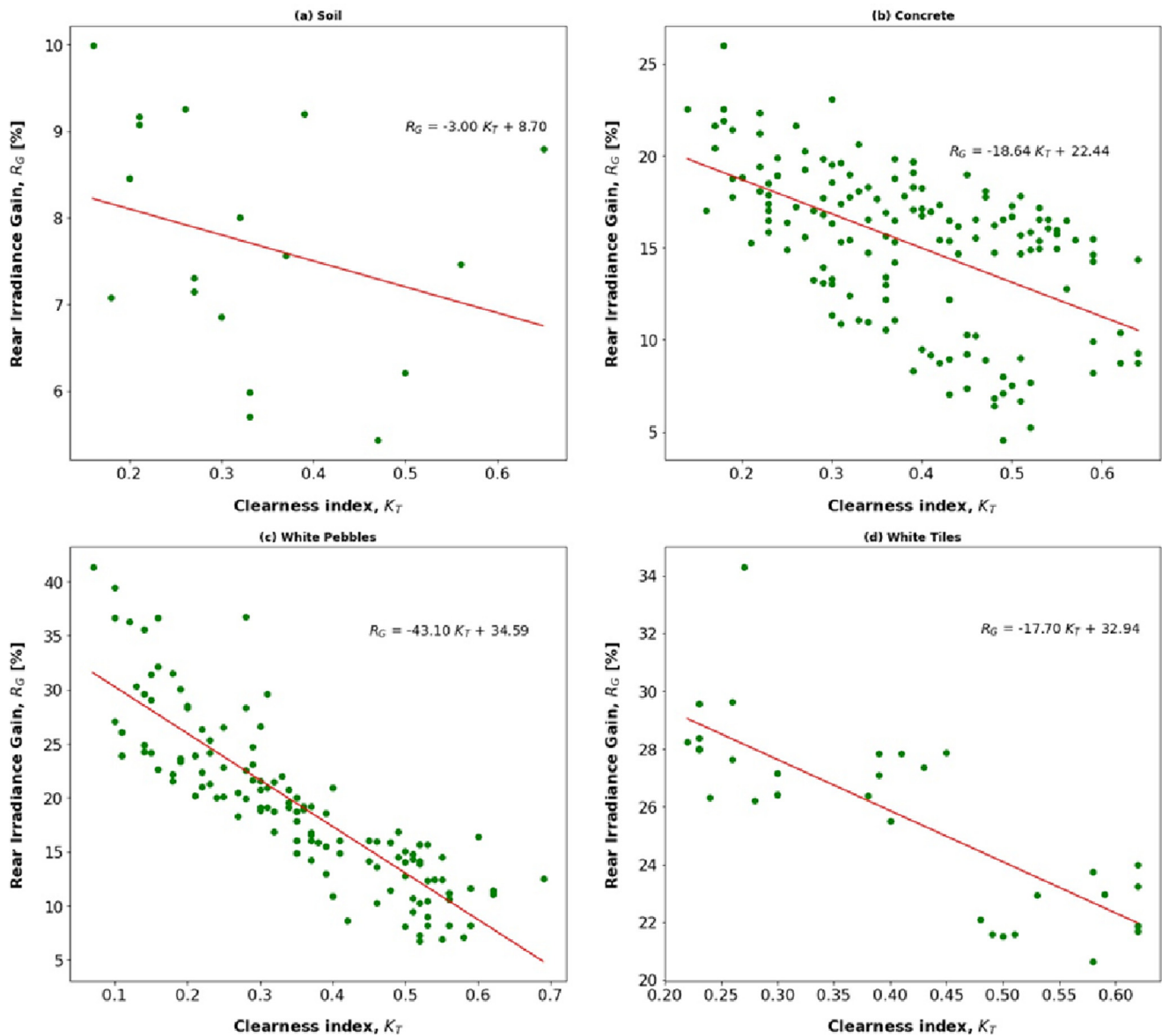


Fig. 8. Rear irradiance gains at different solar altitudes for various ground surfaces, a) Soil, b) White tiles, c) Concrete, and d) White pebbles.

Table 3
Model Summary for linear regression between K_T Vs R_G .

Ground surface	r	R ² [%]	R _{pred} ² [%]	P-value	RMSE [%]	MBE [%]	m	c
Soil	-0.30	9.0	0	0.23	1.27	-0.001	-3.0	8.7
Concrete	-0.55	30.2	28.46	0	3.52	0.001	-18.64	22.44
White Pebbles	-0.86	74.6	73.63	0	3.79	0.005	-43.10	34.59
White Tiles	-0.81	64.9	60.59	0	1.87	0-.001	-17.7	32.94

Table 4
Rear irradiance gains on the sunny and cloudy days.

Ground surface	Sunny Day				Cloudy Day			
	K _T	Mean	Median	S _D	K _T	Mean	Median	S _D
Soil	0.65	8.79	7.12	4.13	0.21	9.17	9.07	1.1
Concrete	0.62	10.38	9.31	3.48	0.23	15.84	15.14	3.56
White Tiles	0.62	23.98	22.78	8.33	0.27	34.31	33.40	5.37
White Pebbles	0.62	11.39	10.57	2.79	0.27	20.46	21.08	2.66

With the changes in solar angle, the amount of rear gain changes diversely in white tiles. This can also be observed in the rear irradiance gain output in Fig. 9. The output is shown for four sunny days. The daily variation in ground reflectance is closely dependent on the solar altitude angle. At lower solar altitudes 10°, the rear irradiance gain is higher, for example (12.5 %) for the soil surface. For white tiles, higher incident angles cause more reflection and the rear irradiance gain increases. At higher altitude angles, the solar incident angle decreases. Therefore, the rear irradiance gain at

During the summer (July), the solar altitude angle varies at a wider range. This phenomenon can be observed in Fig. 9b. For white pebbles, there is a sharp increase in the gain from a solar altitude of

increases (solar zenith angle), the ground reflection also increases. This increase is more prominent for the white pebbles and white tiles ground surfaces.

Apart from ground reflectance, PV installation tilt and mounting height also have an impact on rear irradiance gain and bifacial energy gain. Module geometry, such as optimal tilt angle, is determined by the latitude of the geographic location. The installation height also has an influence up to a specific limit. The change in rear irradiance gain at two different installations of

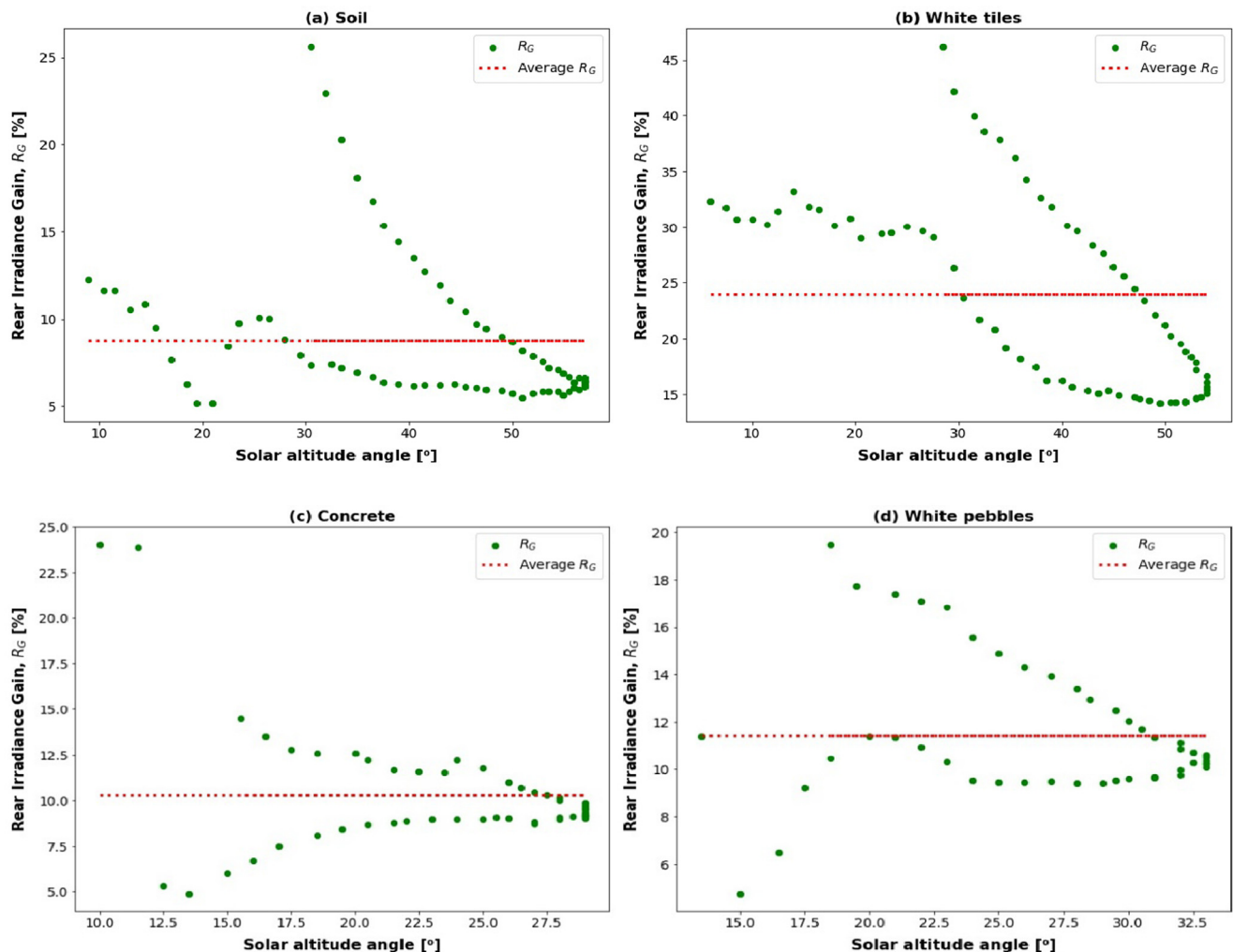


Fig. 9. Rear irradiance gain at different solar altitudes for various ground surfaces, (a) Soil, (b) White tiles, (c) Concrete, and (d) Pebbles.

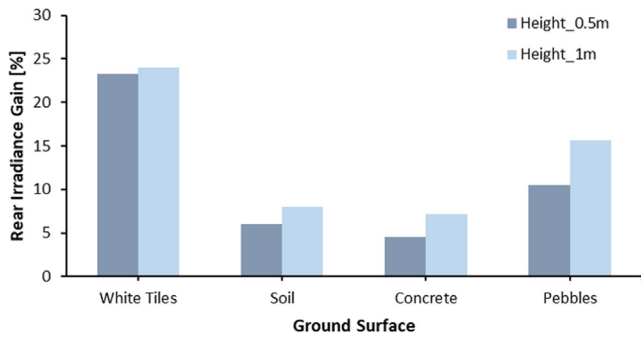


Fig. 10. Rear irradiance gain at a different module installation height of PV.

4.2.3. Annual rear irradiance gains analysis

Long-term measurement data provides confidence in estimating the ranges of gain practically feasible for real-life applications. Hence based on the measured data at different months of the year, the rear irradiance gains and bifacial energy gain are calculated. It is more realistic to specify the rear irradiance gain and bifacial energy gain as a range of values instead of a single value. Therefore, various statistical approaches have been applied to predict the different gain ranges. The first approach is to identify data trends which help to make predictions and gain inside into data. That can be shown with a histogram or frequency distribution plot where the data ranges are divided into bins and put the data values that fall within the same bins. A histogram is helpful in estimating the probability of rear irradiance gain and bifacial energy gain. The taller bar within the histogram shows more data falling into that respective bin.

To understand the results further, an illustration of the normal probability density function (PDF) is helpful. It represents the area under the curve. The width of the normal distribution curve can be defined by the standard deviation. The width of the curve shows that 95 % of the data falls within the ± 2 standard deviation ($\pm 2 \sigma$) around the mean. An illustration of the data’s normal probabil-

ity distribution and its 2-sigma value for rear irradiance gain are presented in Fig. 11 and Table 5, respectively. Among all four-ground surfaces, for soil, the lowest mean gain of 7.7 % and a standard deviation of 1.4 % is observed. At the 2-sigma ($\mu \pm 2 \sigma$) value, the gain is within the 5 % to 10.4 % range. For concrete, the mean gain is 15.3 %. The large area under the bell-shaped curve is within the gain range of 6.8 % to 23.7 %. The mean gain is highest for white tiles (25.6%), followed by white pebbles (19.4%). White pebbles have the highest standard deviation of 7.6 % in irradiance gain, which is understandable from a much wider spread of gain with $\pm 2 \sigma$ from 4.2 % to 34.7 %.

Based on the above analysis, it can be concluded that the rear irradiance gain is lower with the soil surface. Due to maintenance difficulty with long-term testing, the soil has been excluded for further analysis. However, using the empirical model developed between bifacial energy gain and rear irradiance gain, it is possible to estimate the bifacial energy gain for the soil surface.

The rear irradiance gain helps to select the ground surface if enhanced energy yield is expected for any solar PV project. The bifacial energy gain achieved at the ground albedo condition is also essential to examine to justify the deployment of bifacial in place of monofacial PV. A scatter plot showing the relation between rear irradiance gain and bifacial energy gain is shown in Fig. 12, and the regression output is presented in Table 6. A moderately high correlation is observed between rear irradiance gain, R_G and bifacial energy gain, B_G . The R^2 value is 68 % indicating that the 68 % variation in bifacial energy gain can be explained by rear irradiance gain. The root mean square error (RMSE) of the modelled equation show a relative error of 2.9 % between the measured and modelled bifacial energy gain. The MBE is almost negligible. The p-value < 0.05 indicates that the model is highly significant at a 95 % confidence level. The predicted R^2 value is almost equal to the R^2 value, which confirms the model’s reliability in predicting bifacial energy gain. Under all sky conditions (sunny and cloudy days), a close relationship is observed between R_G and B_G . Therefore, this empirical model can be used to estimate bifacial energy gain.

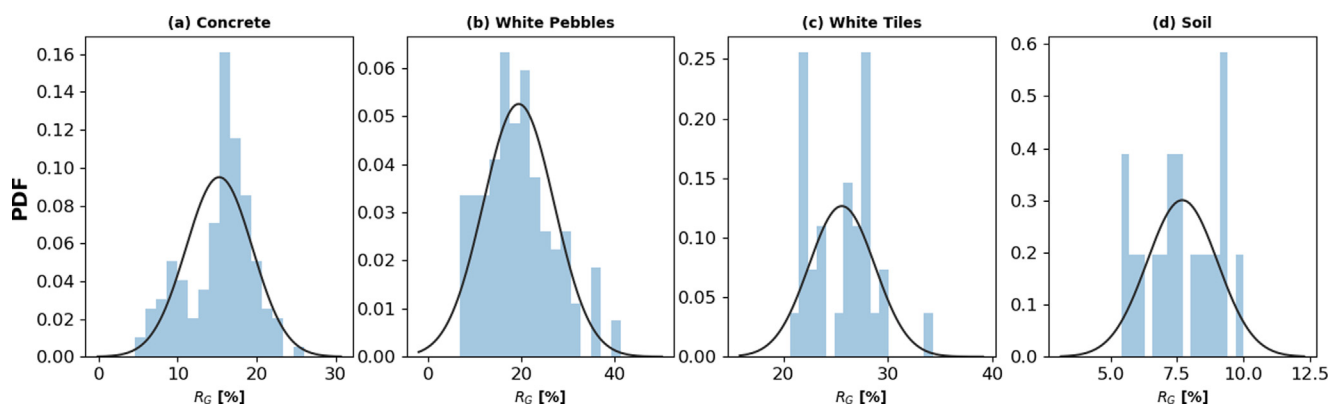


Fig. 11. Rear irradiance gains at different solar altitudes for various ground surfaces, (a) Soil, (b) White tiles, (c) Concrete, and (d) Pebbles.

Table 5
Rear irradiance gains analysis for various ground surfaces showing mean and standard deviation.

Ground surface	μ	σ	$\mu + 1\sigma$	$\mu - 1\sigma$	$\mu + 2\sigma$	$\mu - 2\sigma$
Soil	7.7	1.4	9.1	6.3	10.4	5.0
Concrete	15.3	4.2	19.5	11.1	23.7	6.8
White Pebbles	19.4	7.6	27.1	11.8	34.7	4.2
White Tiles	25.6	3.2	28.8	22.4	32	19.2

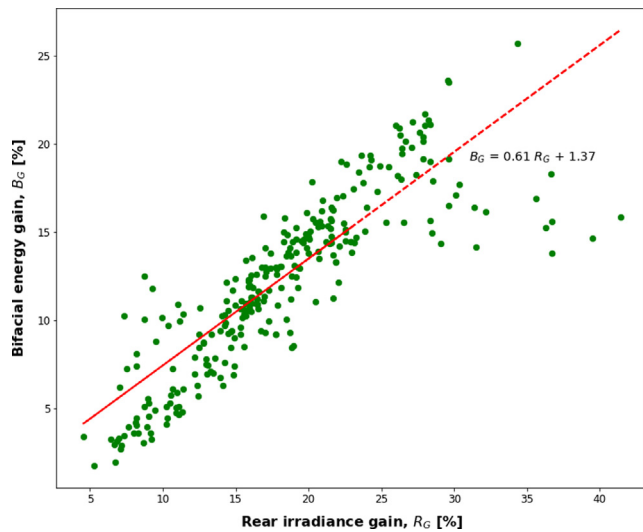


Fig. 12. Scatter plot between bifacial energy gain and rear irradiance gain showing positive correlation.

4.3. Analysis of bifacial energy gain

Bifacial energy gain at various ground reflective surfaces is studied with a histogram plot with normal probability density function and its cumulative distribution (CDF) plot (Fig. 13). CDF helps to depict the probability distribution of the gain ranges. The low standard deviation of bifacial energy gain for white tiles surface shows that the probability is higher that the gain ranges are closer to the mean range of around 19.6%. The narrow histogram indicates less variation in gain for white tiles surface compared to wider variation in concrete and white pebbles surface. The mean ranges of bifacial energy gain (Table 7) for white pebbles are 12.4%, and the $\mu \pm 2\sigma$ value is 2.8% and 22%, respectively, which presents about 95% of the data falling within this range. Similarly, for concrete surfaces, bifacial PV has 2.4%–18.6% more energy gain than monofacial PV. Among all three surfaces, on average, 9% more energy gain was achieved for white tile surfaces in comparison to concrete and pebbles. As can be seen in the CDF plot, for all ground surfaces, the probability of bifacial energy gain falling beyond the 30% range is almost negligible. If the bifacial energy gains are normalised by manufacturer specified STC front side power, the gain will be about 5% higher than the gain shown Table 7.

4.3.1. Analysis of daily power output and irradiance gain on a sunny and a cloudy day

This section analyses the power produced on a sunny and cloudy day (Fig. 14 and 15). The dates of sunny and cloudy days are the 8th and 9th of March for concrete, the 24th and 22nd of July for white tiles, and the 18th and 15th of March for white pebbles. The study indicates that during midday, the highest hourly energy produced crosses 300Wp under all three ground surfaces. The maximum power produced by bifacial PV is 350Wp during midday on a very sunny day in July for white tile’s ground surface. The total effective irradiance at that time was 1070Wh/m². Though the rear irradiance gain achieved by the modules is high during a

cloudy day, the cloudy nature limits the power output. For example, 46Wp power was produced for concrete during mid-day due to a decrease in current. For white tiles and pebbles, these values are about 110Wp and 96Wp, respectively. During the mid-day period from 12 to 2 pm, bifacial PV produce atleast 9% more power than monofacial PV. Overall, the bifacial energy gain is 9.67%–17.67% on a sunny day and 12.3%–26.86% on cloudy days. The results are shown in Table 8.

4.3.2. Correlation study between total effective irradiance and power output

The total effective irradiance and power (P) are strongly correlated (Table 9). The correlation coefficient is 0.998. The R² and predicted R² show the same value of 99.6%, which confirms that the modelled power output can be fully explained by total effective irradiance. The importance of this study is that it is possible to estimate power output using the empirical equation obtained from the linear regression model if the total effective irradiance is known. The RMSE between the measured and modelled power is 5W over 5816 data points, and the mean bias error is only 0.55W. Overall fit is excellent except few data points. This can happen due to the nonlinearity of irradiance, which can be caused by the momentarily shading of the pyranometer. The coefficient value m=0.32 represents that 32% of total effective irradiance is converted into electricity. This 32% can be explained as an irradiance gain factor of bifacial PV, contributed by the module’s front and rear sides. Fig. 16 presents the regression output.

4.3.3. Overall energy yield performance analysis

A meaningful study to understand the performance of bifacial PV is to show the yearly energy mapping, shown in Fig. 17. The missing data in the map indicates system unavailability due to maintenance or I-V tracing testing. The peak generation period occurred from 11 am to 2 pm. The maximum normalised energy produced by bifacial PV was 8.3 kWh/kWp on 20th July’2021 and 24th July’2021. The ground surface for this day was white tiles. For the monofacial module, this was 6.9 and 6.76 kWh/kWp, respectively. The energy mapping for monofacial PV is added in the appendix section (Fig. A1).

To understand the energy mapping more precisely, let’s consider the date window of 27-08-21 to 31-08-21. An example of a sunny day among these days was 28th August 2021. The daily clearness index for the day was 0.56, and the ground surface was concrete. Overall, the hourly energy generation from the bifacial module was more than from the monofacial module. The specific yield for the bifacial module was about 6.7 kWh/kWp, which decreased to the lowest value of 2.2 kWh/kWp on a cloudy day (30th August 2021). The bifacial gain for these sunny and cloudy days was 8.72% and 16.08%, respectively. For the data taken with the ground surface consisting of white pebbles, at the highest clearness index of 0.69 on 20th March’2022, the specific yield was 6.9 kWh/kWp, and the bifacial gain was 10.66%. Though the bifacial gain was maximum for all three-ground surface during a cloudy day with the same K_T value, the specific yield produced for both bifacial and monofacial PV on all those days were below 3 kWh/kWp. Example days are 6th September for concrete, 23rd September for pebbles, and 9th August for white tiles. All these

Table 6
Model Summary for linear regression between B_G Vs R_G.

Model	r	R ² [%]	R ² _{pred} [%]	P-value	RMSE [%]	MBE [%]	m	c
B _G Vs R _G	0.82	68	67	0	2.9	-0.08	0.61	1.37

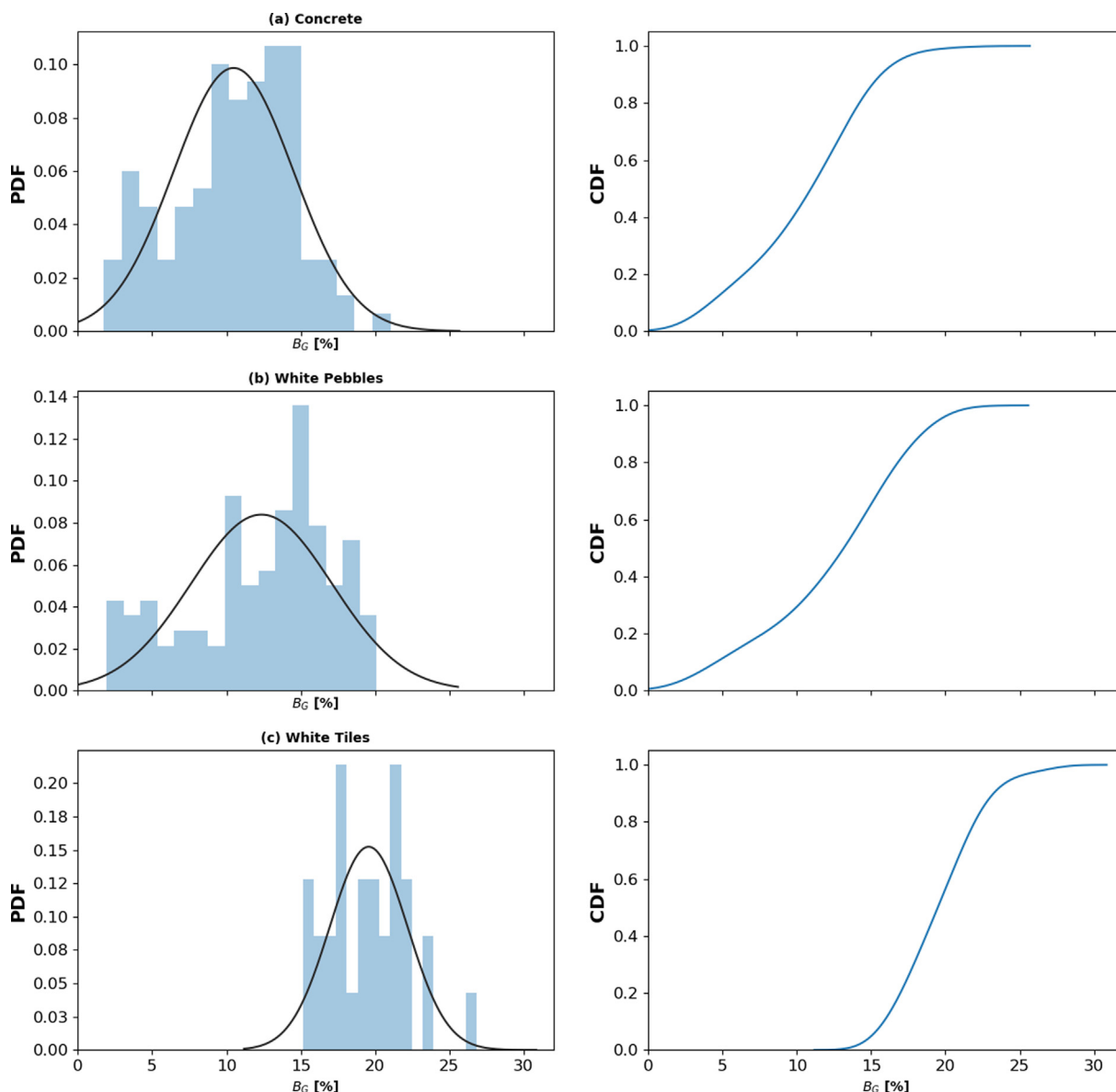


Fig. 13. Overall bifacial energy gain frequency distribution plot for concrete, white pebbles, soil and white tiles ground surface.

Table 7
Bifacial energy gains analysis at various ground reflective surface showing mean and standard deviation.

Ground surface	μ	σ	$\mu + 1\sigma$	$\mu - 1\sigma$	$\mu + 2\sigma$	$\mu - 2\sigma$
Concrete	10.5 %	4.1 %	14.5	6.4 %	18.6 %	2.4 %
White Pebbles	12.4 %	4.8 %	17.1	7.6 %	21.9 %	2.8 %
White Tiles	19.6 %	2.7 %	22.2	16.9 %	24.9 %	14.3 %

days have a similar K_T value of 0.22. The highest specific yield was achieved on 9th August by white tiles, which are 2.6 kWh/kW_p.

The annual energy performance is shown in Fig. 18. Yearly overall energy production by bifacial PV was 298 kWh which is 11 % more than the total energy production by monofacial PV (270 kWh). The Fig. 18 shows daily net energy output from July'2021 to May'2022. Seasonal variations, such as high energy yield in May and July due to high solar irradiation, are visible. The highest energy was recorded on 20th July, producing 2.79 kWh of energy on the day. The rear irradiance gain and bifacial energy gain on the day were 22 % and 13 %, respectively.

5. Bifacial energy gain comparison of PV plant at various scales in PVsyst

It is understandable that bifacial PV performance depends on the number of modules. The small row benefits from an open non-shaded region and less ground coverage ratio and overestimates the performance gain than the utility-scale plant. During this research, to understand the variation of bifacial energy gain with respect to the system size, several simulations were run in PVsyst across various locations in the UK, namely Pilton, Cottingham, Bridlington, Horbury, Harrogate South, Glenlee and Irvine. The

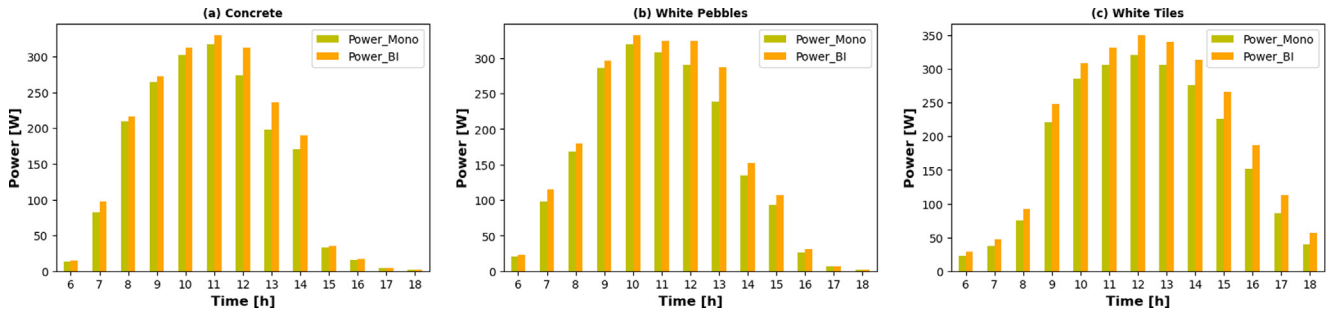


Fig. 14. Power output for the various ground surface on a sunny day, (a). concrete, (b) white pebbles and (c) white tiles.

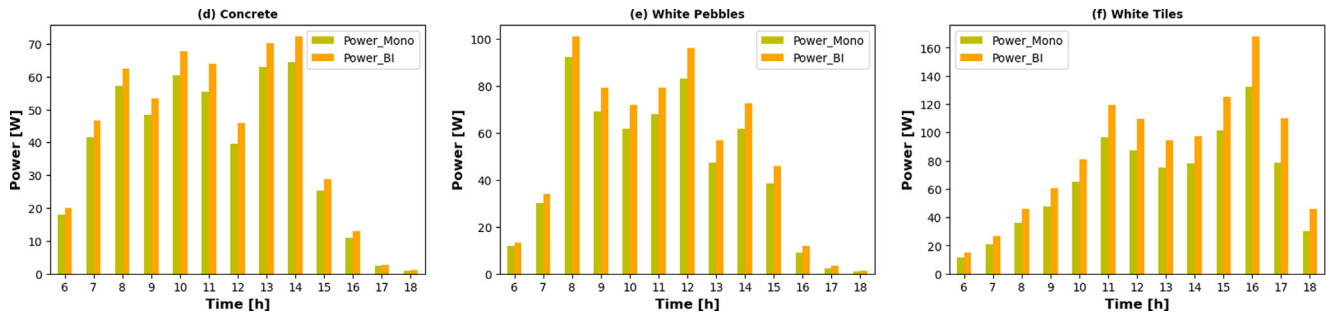


Fig. 15. Power output for the various ground surface on a cloudy day, (a). concrete, (b) white pebbles and (c) white tiles.

Table 8
Bifacial energy gain analysis on a single sunny and cloudy day

Albedo	Sunny Day			Cloudy Day		
	Mean	Median	SD	Mean	Median	SD
Concrete	9.67	7.7	7.19	12.3	12.01	2.28
White tiles	17.67	15.56	8.42	26.86	25.81	4.43
Pebbles	10.31	8.95	6.41	15.53	16.23	3.10

Table 9
Model Summary for linear regression between Power Vs G_T .

Model	r	R ² [%]	R _{pred} ² [%]	P-value	RMSE [W]	MBE[W]	m	c
P _m Vs G _T	0.99	99.6	99.6	0	5	0.55	0.32	2.85

sites are potential PV candidates at different topologies, such as flat ground and hillside. The assessment was conducted at multiple capacities categorised as small, medium, and large-scale PV arrays, ranging from 43.2 kW_p to 56.19 MW_p. Each simulation is carried out with the near shading scene subject to place, taking nearby structures and trees into account. System losses were considered during the simulation following the guideline based on the consultation with the expert in the field. Some of the loss parameters are thermal loss factor: 29 W/m²K, soiling loss: 1 %, Ohmic loss: 1.5 % and module mismatch loss: 0.3 %, light-induced degradation loss: 1.6 %. Meteonorm 8.0 typical meteorological year (TMY) data was used for simulation, which provides hourly data at 4 %–6 % annual variability. The PVSyst simulations were run in batch mode at a tilt angle of 20°–90°, ground clearance height of 1m and a pitch of 8–9m. The key findings of simulations are discussed below.

Figs. 19 and 20 present bifacial energy gain at various module tilts and ground albedo. The installation angle of PV is latitude-dependent parameter. The bifacial energy gain increases with module tilt. Vertically PV has the highest bifacial energy gain of 22 %–47 %. The maximum gain achieved for vertical PV at a ground albedo of 0.2 is 25 %. At 90°, the reason for higher gain is the benefits of uniform distribution of irradiance on both the front and

rear sides of bifacial PV, whereas the energy produced by monofacial PV decreases considerably.

At albedo of white pebbles and white tile, the bifacial energy gain is much higher. The higher bifacial energy gain of vertical solar PV makes it an appropriate choice for building (such as building façades) and highway (for example, noise barrier) applications. Regardless of the system size, the bifacial energy gain increased linearly with ground albedo. For the module tilt of 45°, the highest gain for ground albedo 0.5–0.6 is 9.72 %–12 %. For ground albedo of 0.3–0.40, the bifacial energy gain was 6.75 %–9 %.

The PVSyst simulation results are consistent with the field data result regardless of the system size. For example, at a ground albedo of 0.3 (albedo of concrete), an installation angle of 45°, the bifacial energy gain from the simulation was 7 %. For a similar condition, the average bifacial energy gain achieved from the test site was 10.5 %. If compared with data from around the world, on 12 different locations (Table 1), the finding is that the gain for the same ground albedo was 10.4 % in a test site in Italy. Another example can be a ground albedo of 0.4–0.6 (albedo of white pebbles). The gain from the simulation result was 8 %–11 %, whereas the average measured gain was 12.4 %, and the reported gain was 8.9 %–11.2 % in a test site in France and Denmark. Overall, the mea-

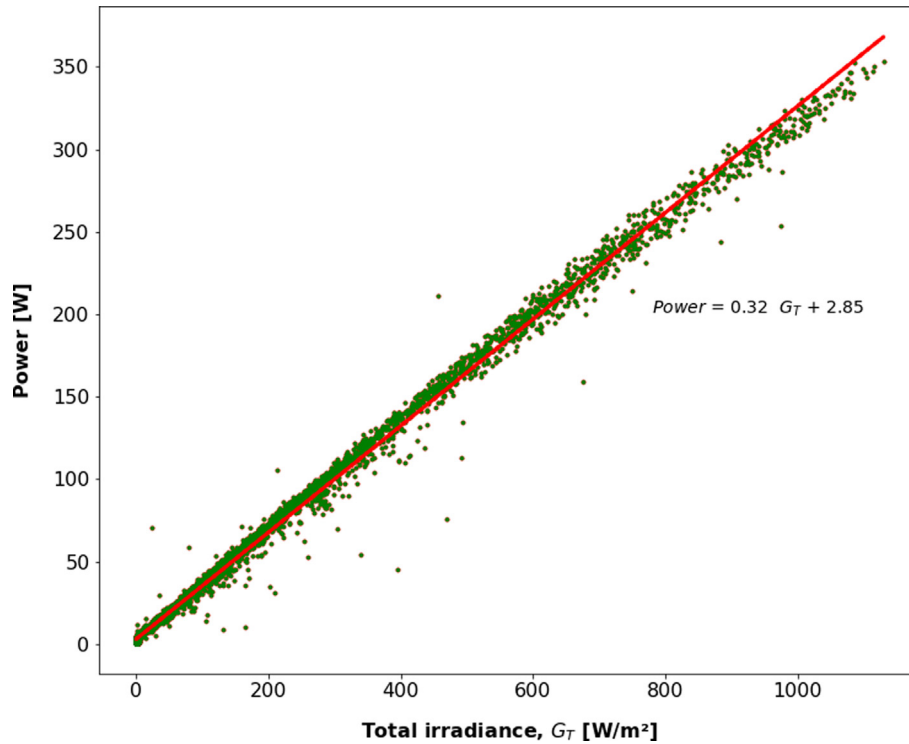


Fig. 16. The Scatter plot between power and total irradiance shows a strong positive correlation.

sured bifacial energy gain correlated well with the PVSyst results, and the bifacial energy gain reported worldwide.

6. Case study on economic analysis of bifacial project

Once a technology has been identified as technically feasible, it is important to assess its economic feasibility. The same applied to bifacial PV. In this research, a case study has been built for a potential PV location in North Ayrshire, UK. The identified site has a PV potential of an annual generation of 7645 MWh by monofacial PV and 8074 MWh by bifacial PV for a total install capacity of 7.025 MW_p. Various approaches are available for economic appraisal. Here two standard measures have been considered for the economic analysis of the project.

1. Net present value (NPV)
2. Levelized cost of electricity (LCOE) which can be calculated as [36],

$$LCOE = \frac{CAPEX + \sum_{n=1}^N \frac{OPEX}{(1+r)^n}}{\sum_{n=1}^N \frac{E_0(1-D)^n}{(1+r)^n}} \quad (21)$$

Here,

CAPEX = Total investment cost

OPEX = Annual operation and maintenance cost

r = Discount factor

D = Degradation rate

E = Energy yield

N = Project lifetime

The net present value (NPV) indicates the project's lifetime discounted benefit. For a project to be viable, the discounted benefits

must exceed the discounted cost. The net cash flow (NCF) is discounted and summed up to get the NPV. The levelized cost of electricity is the ratio of the total discounted cost and the total discounted energy production over the project's lifetime. LCOE calculation assumption was made based on the guideline for PV cost calculation which has been further confirmed by the expert in the PV industry [36]. A calculation tool has been developed in Excel to perform the LCOE study. The CAPEX was considered £1032/kW_p, and OPEX £6/kW_p. The bifacial PV energy yield is assumed under the albedo of white pebbles, and the reflectance, ρ, is assumed to be at the lower end of 0.35 to avoid any overestimation of LCOE reduction. However, the reflectance of white pebbles can be as high as in the range of 0.5–0.6. The cost of white pebbles is included with the capital cost for bifacial PV. The discount factor is 5%. The O&M cost growth rate is considered 2% per year.

In this study, the energy produced is assumed to be used on-site, which causes potential savings in electricity purchase costs from the grid. For medium-scale systems, the electricity purchase cost is 16.51p/kWh [37] for the non-domestic sector, with a 2% annual increment. The annual degradation rate for bifacial PV is 0.45%, and for monofacial, that is 0.55%. The currency for LCOE is shown in the British penny (p). The LCOE of bifacial PV is 7.15 p/kWh, less than 8% LCOE of monofacial PV. If the higher albedo of white pebbles is considered, the LCOE further lowered to 7.03 p/kWh (ρ=0.5) and 7.11 p/kWh (ρ=0.4), which indicates white pebbles have the potential to reduce the LCOE by 0.76p/kWh than monofacial PV which can be economically beneficial over a bifacial PV project lifetime of 30 years. For a low albedo ground surface such as grass (ρ=0.2), the LCOE for bifacial PV is 7.28p/kWh. The LCOE calculation summary is shown in Table 10.

6.1. Sensitivity analysis of LCOE

The LCOE depends on five significant variables: capital cost, operational cost, annual energy production, discount factor and degradation of the module. A sensitivity analysis is conducted for bifacial PV to explore the dependence of these variables Fig. 21.

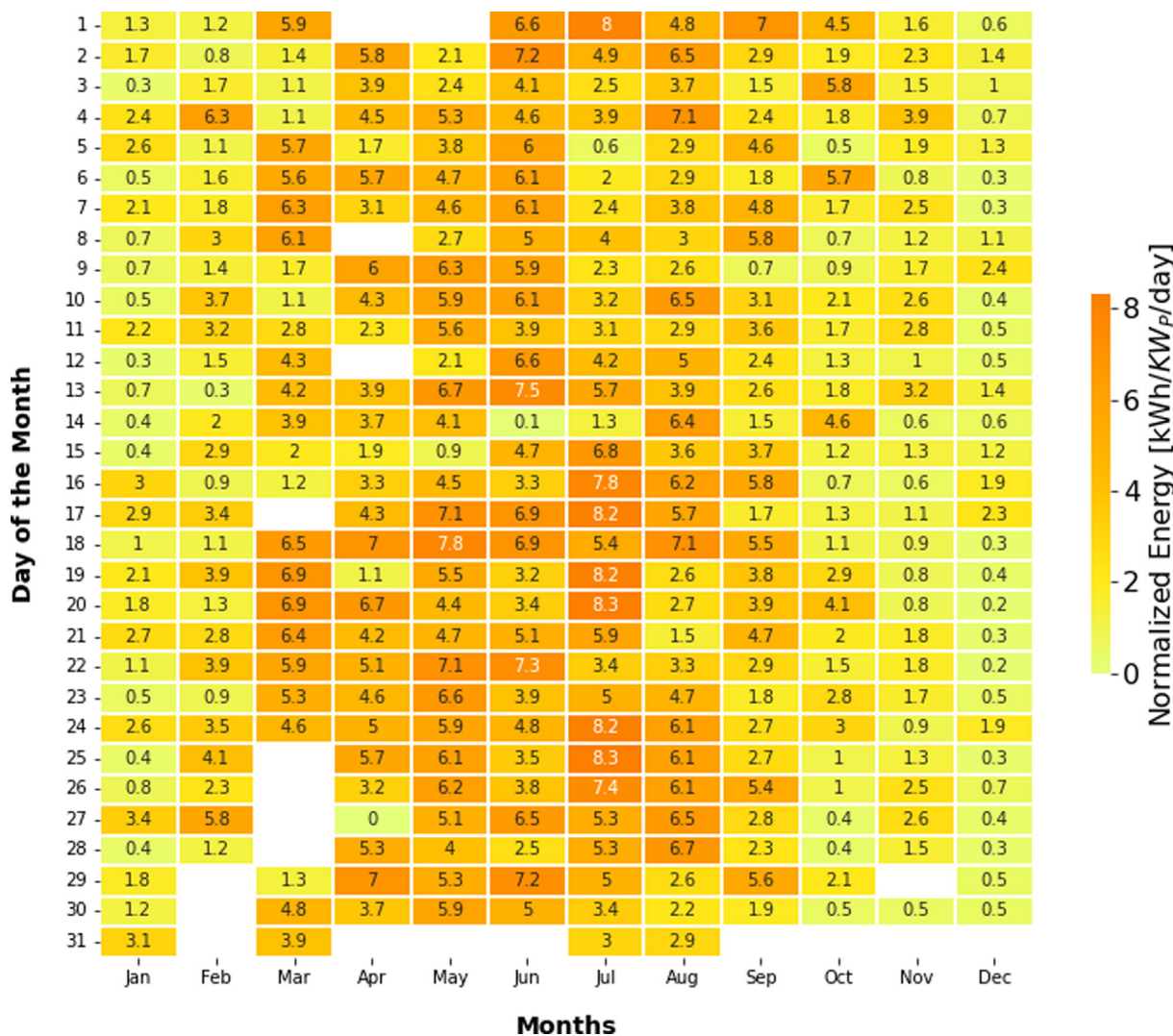


Fig. 17. Annual energy heatmap of bifacial PV

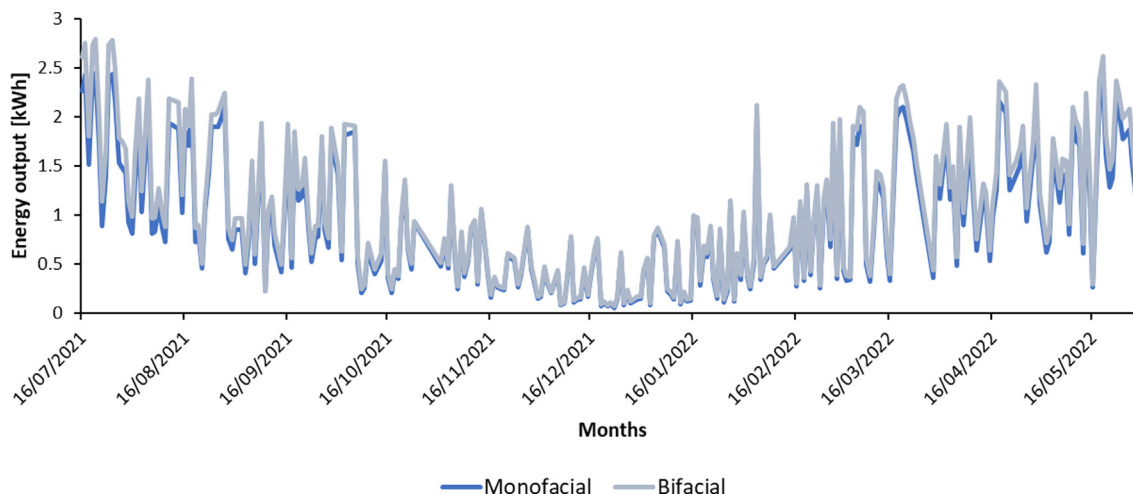


Fig. 18. Annual energy production of bifacial and monofacial PV.

The midpoint value of 0% shows the value shown in Table 6.11, where the LCOE is 7.15p/kWh. The vertical axis represents the LCOE at relative changes of input variables in the range of +30% to -30%, as shown in the horizontal axis. The analysis shows that

the resulting LCOE is highly sensitive to energy yield. For bifacial energy, higher energy yield can be achieved by using a high reflectance ground surface. However, the increase in CAPEX can raise the LCOE. Therefore, the cost of ground-reflective material must go

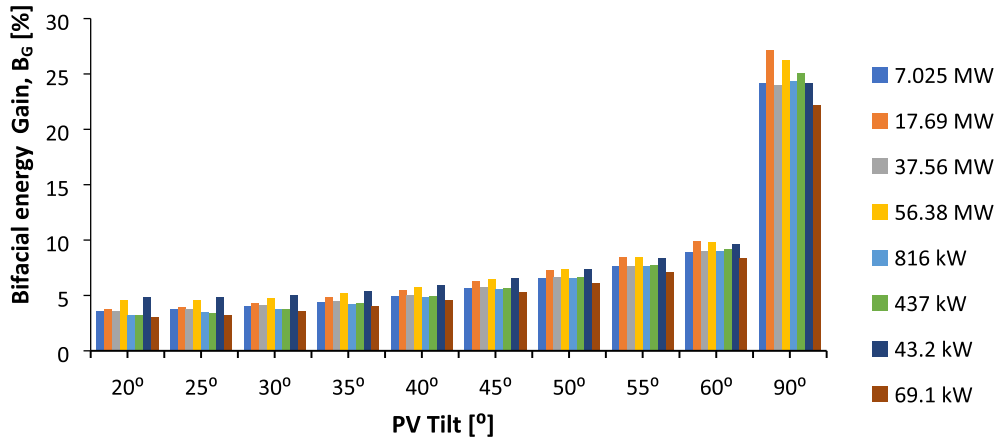


Fig. 19. Bifacial energy gain at various PV installation tilt.

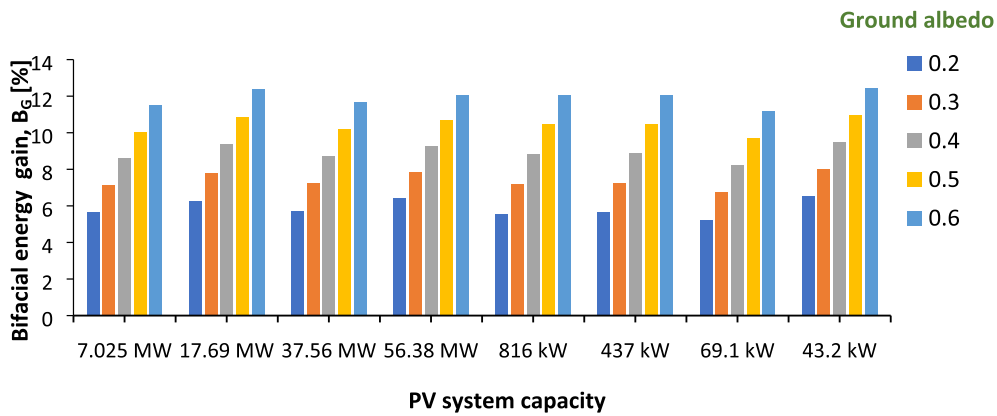


Fig. 20. Bifacial energy gain at different ground albedo.

Table 10
LCOE calculation summary.

Parameters	Bifacial PV	Monofacial PV
System size	7.025 MW _p	7.025 MW _p
Annual energy production	8074 MWh	7645 MWh
CAPEX	£7249800	£7637880
OPEX	£42150	£42150
LCOE	7.15 p/kWh	7.79 p/kWh
Net present value, NPV	£16m	£13m
Payback period	Seven years	Seven years

down to achieve the benefits of deploying a high reflectance surface. OPEX and degradation have comparatively less impact on LCOE. An extended project lifetime spreads the cost over longer periods; therefore, the LCOE decreases. The higher discount factor seems to minimise the benefits of an extended lifetime.

7. Discussion and conclusion

This paper discusses the findings of the field test result conducted at the University premises. Bifacial PV’s electrical perfor-

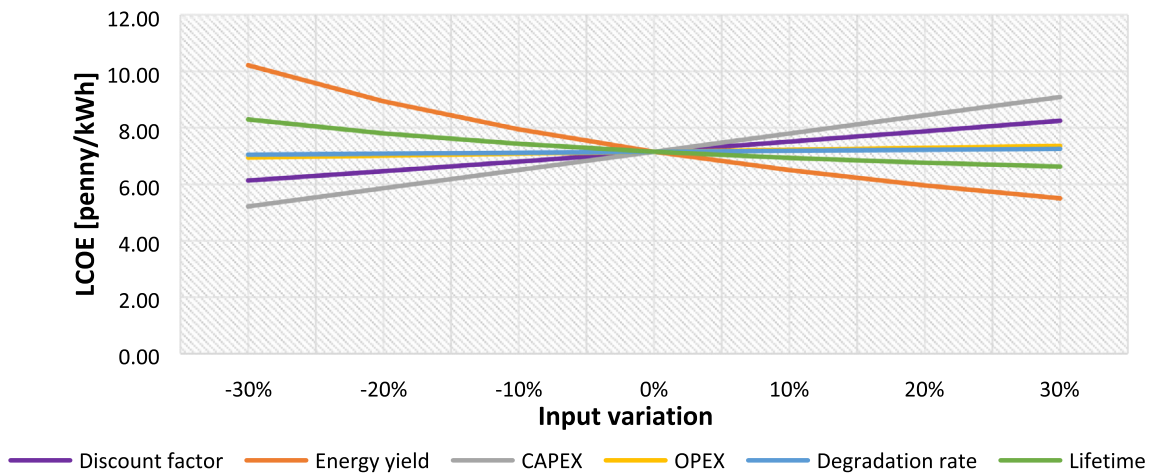


Fig. 21. Sensitivity analysis of LCOE

mance is measured and compared using the monofacial photovoltaic system as a reference. Ground albedo affecting the performance of PV is evaluated. A comparison of bifacial energy gain at different ground albedo conditions using the field data is shown. A detailed analysis is conducted for 12 months to observe the energy yield improvement in bifacial PV. A data analysis tool has been developed to evaluate the field data and monitor the performance. It has also been examined how the enhanced ground albedo contributes to the reflected irradiance received at the rear side of the module. The significant contribution of this research is that six empirical models are presented based on the findings of this research. These models are essential for designing and estimating bifacial solar PV systems' energy gain potential. It is possible to estimate power output using the empirical equation obtained using linear regression in this research. The key findings are:

- The correlation studies between rear gain and clearness index, K_T showed that white pebbles and white tiles have the highest dependency on clearness index among four reflective ground surfaces. Soil showed weak dependency on K_T , whereas a moderate correlation is observed for concrete surfaces.
- A moderately high correlation is observed between the bifacial energy gain and rear irradiance gain, indicating that the high energy gain of bifacial PV strongly depends on the reflectance of the near-ground surface underneath the bifacial PV module.
- The power output of bifacial PV shows a strong correlation with total effective irradiance and the irradiance gain factor was 0.32 such that 32 % of total irradiance (including global tilted irradiance at the front side and the global reflected irradiances at the rear side) converted into electricity.
- A detailed statistical analysis is presented to quantify the rear irradiance and bifacial energy gain at various ground reflective surfaces. Based on the annual rear irradiance gain analysis, the highest gain range is found for white pebbles and white tiles ground surface (>30 % gain) and lowest for soil surface within the 5 %–10 % range. For concrete, the maximum gain observed was >20 %.
- On a daily basis, sunny days offer lower rear irradiance gain and energy gain than cloudy days due to less diffuse irradiance component in the total irradiance received by the module. It has also been found regardless of the ground's reflective surface, the probability is very low that the bifacial energy gain is more than 30 %. However, for vertical PV, the bifacial energy can be considerably higher, which is shown in the simulation results.
- The ranges of bifacial energy gain within the ± 95 % confidence interval are determined. The highest-level bifacial energy gain was achieved from the white tiles (14.3 %–25 %). The next highest level of bifacial energy gain was achieved from the pebbles (2.8 %–22 %) and the amount of gain obtained from the concrete (2.4 %–18.6 %). The results show consistency with the output of the PVSyst simulations results and the data reported from around the world. The normalised bifacial energy gain will be about 5 % higher than these gain.
- On a daily basis, during the mid-day period from 12 to 2 pm, bifacial PV produce 9 % to 23 % more power than monofacial PV. Overall, the bifacial energy gain is 9.67 % to 16 % on a sunny day and 12 %–25.66 % on cloudy days. The highest energy was recorded on 20th July, producing 2.79 kWh energy. The rear irradiance gain, and bifacial energy gain were 22 % and 13 %, respectively.
- Based on the case study run on the LCOE of a bifacial PV project (7MW_p installed capacity) is calculated at 7.15p/kWh, which is 8 % less than the LCOE of monofacial PV. By enhancing the energy generation at higher ground surface reflectance of 0.5, LCOE can be reduced to 7.03p/kWh.

The massive deployment of bifacial technology globally will depend on field test results and their validation. Three core parameters: rear irradiance gain, bifacial energy gain, and power output, are crucial to understand the performance of bifacial PV. To win the investors' confidence, it requires more field data, set standards, testing procedures and modelling tools to reduce the uncertainty of bankability. The contribution of this research is the correlation study and development of the various empirical model between (i) clearness index and rear irradiance gain; (ii) rear irradiance gain and bifacial energy gain; (iii) total effective irradiance and the power output. These empirical models help to explore the relationship between variables under consideration and make a prediction about bifacial PV performance. Moreover, the findings of this research can provide an important indication of the expected outcome from the PV system installation in countries with high latitude and low clearness index and receive a significant portion of diffuse irradiances, such as the UK, Germany, Westcoast of Canada, and the Netherlands. These countries can benefit more from rear irradiance gain due to increased ground albedo. The methodology presented in this research can be applied for other locations as well such as countries in equator or tropics. The strength of this research is its long-term data which is a major demand in bifacial PV research. The detailed analysis provides valuable insight to ascertain how much bifacial energy gain is practically feasible and how can its full potential be achieved by using the enhanced ground surface. The outcome of this research is important in bridging the gap between expectation versus reality about the performance of this new technology.

Finally, it is understandable that bifacial PV performance depends on the number of modules. This research can be an important benchmark in scaling up the solar PV system at a large scale by considering this small system as a reference. The findings of this research can be applied to design and validate overall bifacial PV system performance, which will help to estimate the expected bifacial energy gain, energy production and overall performance of the system. Based on the BPV gain performance at four different surfaces, it can be said that regardless of the surface reflectance, the bifacial PV is beneficial over monofacial PV. Soil being a natural ground surface, the reflectance of it depends on the soil type, module installation location. To utilise the full potential of bifacial PV, the ground albedo of at least 0.3 to 0.35 is recommended. Grey or white concrete can be recommended to maximise the irradiance gain in a rooftop PV system. When selecting concrete, it is essential to check the constituent material that the concrete is made of. A study on 45 different concrete mixes showed that concrete made of slag cement has higher reflectance than concrete made of ordinary cement. However, white concrete can exceed the reflectance of more than 0.7 [38]. White tiles are also recommended for a rooftop PV-based system. Though the white tiles offer the highest bifacial energy gain, considering the cost constraints, these are not recommended for commercial-scale ground-mount PV. Another point is that using white tiles or concrete for the ground mount system will compromise the ecology. However, concrete can still be used for the small-scale setup for the ground mount system. High reflectance surfaces such as white tiles and pebbles have already gained attention for cool roof surfaces. Integrating solar PV in rooftop systems can be beneficial in reducing energy load from the grid while simultaneously decreasing cooling demand and reducing the urban heat island effect [39]. Special consideration should be given to roof cleaning to prevent reflectance reduction. Pebbles are considered the most suitable option if reflected augmentation is considered for commercial-scale PV system installation. The size of the white pebbles has an impact on the reflectance. A study on five different pebble sizes showed that the pebbles with the finest size (4 mm) had the highest reflectance, 0.62 in the lab and 0.44 in field

measurement [40]. Therefore, attention should be given to their sizes when selecting white pebbles. At least the pebble size of 10mm ($\rho=0.4$) is recommended. One of the biggest challenges in deploying high-reflecting surfaces at a commercial scale is the cost. Though higher reflectance can increase the bifacial energy gain significantly, still the cost is not low enough to justify their usage. There is a need for a combined effort from the PV industry, builders, and suppliers of high reflectance ground materials to reduce their costs to enable the use of the bifacial PV at its maximum capacity.

Author contributions

Conceptualisation: T. M, M. S. G and M. A; Methodology: M. A, T. M and M. S. G; Formal Analysis: M. S. G, T. M and M. A; Coding: M. A, T. M; Resources: T. M, M.S. G and M. A; Data curation: M. A, T. M and M.S. G; Writing—original draft preparation: M. A; Writing—review and editing: T. M, M. S. G and M. A; Supervision: M. S. G, T. M.

Funding

This project is being run in collaboration with four partners: Energy Technology Partnership (ETP), Scotland; Wood Group, UK Ltd; Heriot-Watt University and Edinburgh Napier University, UK.

Data availability

The data that has been used is confidential.

Declaration of Competing Interest

The authors declare that they have no known competing financial interests or personal relationships that could have appeared to influence the work reported in this paper.

Acknowledgements

Authors are grateful to Absolute Solar and Wind (ASAW) for technical support. We would also like to thank Edinburgh Napier University and Wood Group, UK Ltd, for their guidance and support.

Appendix A

See Fig. A1 and Table A1, A2 and A3.

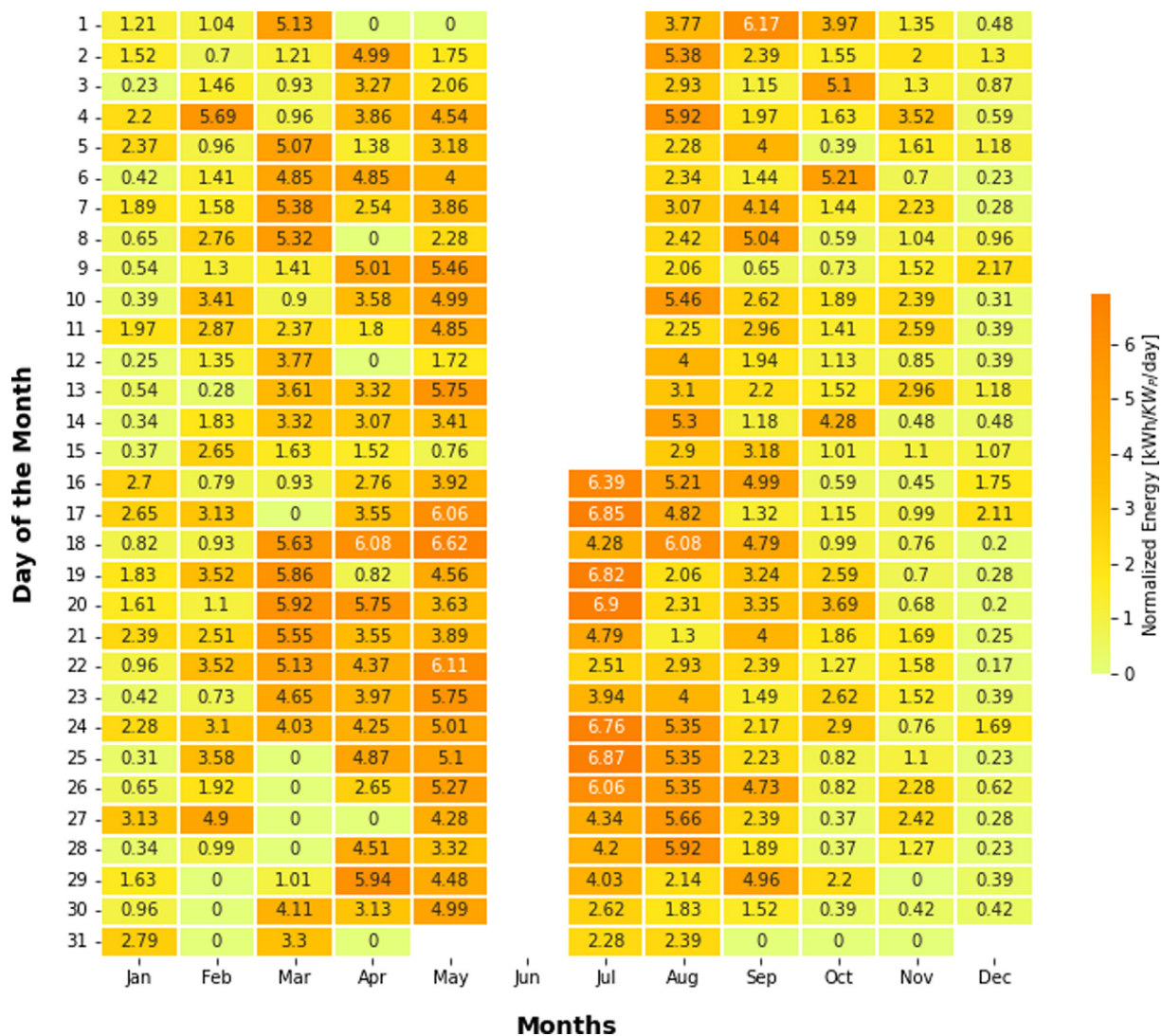


Fig. A1. Annual energy heatmap of monofacial PV.

Table A1
Data measurement schedule.

Timeline	Albedo	Height	Tilt
1st cycle			
June'01–June'15	Concrete	0.5m	45°
June'16–June'22	Concrete	1m	45°
June'23–June'24	Concrete	1m	30°
June'25–June'29	Soil	1m	30°
June'30–July'06	Soil	1m	45°
July'07–July'13	Soil	0.5m	45°
July'14–July'22	White tiles	0.5m	45°
July'07–July'13	White tiles	1m	45°
2nd cycle			
July'30–August'05	White tiles	1m	45°
August'06–August'12	White tiles	0.5m	45°
August'20–August'26	Concrete	0.5m	45°
August'27–August'31	Concrete	1m	45°
September'02–September'06	Concrete	1m	60°
September'08–September'12	Pebbles	1m	60°
3rd cycle			
September'13–October'3rd	Pebbles	1m	45°
October'4th–October'24th	Pebbles	0.5m	45°
October'25th–November'14th	Concrete	0.5m	45°
November'15th–December'5th	Concrete	1m	45°
December'6th–December'31st	Pebbles	1m	45°

Table A2
Specification of monofacial solar panel.

Parameters	STC	NMOT
Maximum Power Pmax [W]	355	266
MPP Voltage V_{mpp} [V]	35.7	33.5
MPP Current I_{mpp} [A]	9.95	7.93
Open circuit voltage V_{oc} [V]	41.4	39.0
Short circuit current I_{sc} [A]	10.65	8.56
Module efficiency [%]	20.7	
Operating temperature [°C]	−40 ~ +90°C	
Maximum system voltage [V]	1000	
Temperature coefficient		
NOCT	42 ± 3 °C	
P_{mpp}	−0.36 %/°C	
V_{oc}	−0.26 %/°C	
I_{sc}	0.03 %/°C	

Table A3
Specification of bifacial solar panel

Parameters	STC	BiFi100	BiFi200	NMOT	BiFi100	BiFi200
Maximum Power Pmax [W]	335	355	375	251	266	281
MPP Voltage V_{mpp} [V]	34.1	34.1	34.1	32.0	32.0	32.0
MPP Current I_{mpp} [A]	9.83	10.41	11.0	7.84	8.31	8.78
Open circuit voltage V_{oc} [V]	40.7	40.7	40.7	38.2	38.2	38.2
Short circuit current I_{sc} [A]	10.34	10.95	11.57	8.31	8.80	9.29
Module efficiency [%]	19.6	20.7	21.9			
Operating temperature [°C]	−40 ~ +90°C					
Maximum system voltage [V]	1000					
Temperature coefficient						
NOCT	42 ± 3 °C					
P_{mpp}	−0.36 %/°C					
V_{oc}	−0.27 %/°C					
I_{sc}	0.03 %/°C					

References

[1] A. Di Paula, Saudi Arabia Gets Cheapest Bids for Solar Power in Auction, Bloomberg, 2017, [Online], Available: <https://www.bloomberg.com/news/articles/2017-10-03/saudi-arabia-gets-cheapest-ever-bids-for-solar-power-in-auction?leadSource=verify> wall.

[2] P. Tillmann, K. Jäger, C. Becker, Minimising the levelised cost of electricity for bifacial solar panel arrays using Bayesian optimisation, Sustain. Energy Fuels (2019).

[3] R. Kopecek, J. Libal, Bifacial photovoltaics 2021: status, opportunities and challenges, Energies (2021).

[4] I. Araki, M. Tatsunokuchi, H. Nakahara, T. Tomita, Bifacial PV system in Aichi airport-site demonstrative research plant for new energy power generation, Sol. Energy Mater. Sol. Cells (2009).

[5] G.J. Faturrochman, M.M. de Jong, R. Santbergen, W. Folkerts, M. Zeman, A.H.M. Smets, Maximizing annual yield of bifacial photovoltaic noise barriers, Sol. Energy (2018).

[6] I. Shoukry, J. Libal, R. Kopecek, E. Weffringhaus, J. Werner, Modelling of bifacial gain for stand-alone and in-field installed bifacial PV modules, Energy Proc. (2016).

- [7] M. Chen et al., Improvement of the electricity performance of bifacial PV module applied on the building envelope, *Energy Build.* (2021).
- [8] J.N. Alexander, A.M.P. Granlund, The influence of module tilt on snow shadowing of frameless bifacial modules, in: 36th European Photovoltaic Solar Energy Conference and Exhibition (EU PVSEC), 2019, pp. 1650–1654.
- [9] J.V.N. Riedel-Lyngskær, D. Berrian, D. Alvarez Mira, A.A. Protti, S. Thorsteinsson, P.B. Poulsen, J. Libal, Large-scale bifacial PV test field performance compared to simulations using commercially available software, research-based and open source tools, in: 37th European Photovoltaic Solar Energy Conference and Exhibition (EU PVSEC), 2020, pp. 1324–1329.
- [10] X. Sun, M.R. Khan, C. Deline, M.A. Alam, Optimization and performance of bifacial solar modules: a global perspective, *Appl. Energy* (2018).
- [11] C. Pike, E. Whitney, M. Wilber, J.S. Stein, Field performance of south-facing and east-west facing bifacial modules in the Arctic, *Energies* (2021).
- [12] M.S.J. Bonilla Castro, M. Herz, C. Monokroussos, Energy yield comparison between bifacial and monofacial PV modules: real-world measurements and validation with bifacial simulations, in: 35th EUPVSEC, Brussels, 2018.
- [13] M.S.J. Saal, J. Bonilla Castro, Energy yield comparison between bifacial and monofacial PV modules : real world measurements in desert climate, in: 36th EU PVSEC, Marseille, 2019.
- [14] G.M. Tina, F. Bontempo Scavo, L. Merlo, F. Bizzarri, Comparative analysis of monofacial and bifacial photovoltaic modules for floating power plants, *Appl. Energy* (2021).
- [15] W. Gu, T. Ma, S. Ahmed, Y. Zhang, J. Peng, A comprehensive review and outlook of bifacial photovoltaic (bPV) technology, *Energy Convers. Manage.* (2020).
- [16] G.M. Tina, F.B. Scavo, S. Aneli, A. Gagliano, Assessment of the electrical and thermal performances of building integrated bifacial photovoltaic modules, *J. Clean. Prod.* (2021).
- [17] H. Nussbaumer, M. Klenk, M. Morf, N. Keller, Energy yield prediction of a bifacial PV system with a miniaturized test array, *Sol. Energy* (2019).
- [18] International Energy Agency, Bifacial Photovoltaic Modules and Systems: Experience and Results from International Research and Pilot Applications, 2021.
- [19] J.E. Castillo-Aguilella, P.S. Hauser, Multi-variable bifacial photovoltaic module test results and best-fit annual bifacial energy yield model, *IEEE Access* (2016).
- [20] M. Gul, Y. Kotak, T. Muneer, S. Ivanova, Enhancement of albedo for solar energy gain with particular emphasis on overcast skies, *Energies* (2018).
- [21] K. Lee, Performance Modeling and Testing of Bifacial PV Systems, CFV, 2019. [Online]. Available: https://www.firstsolar.com/-/media/First-Solar/Technical-Documents/Bifacial-Documents/CSA_Performance-Modeling-and-Testing-of-Bifacial-PV-Systems_Kyumin-Lee.ashx.
- [22] H.E. Beck, N.E. Zimmermann, T.R. McVicar, N. Vergopolan, A. Berg, E.F. Wood, Present and future köppen-geiger climate classification maps at 1-km resolution, *Sci. Data*, 2018.
- [23] J.A. Duffie, W. A. Beckman, *Solar Engineering of Thermal Processes*, fourth edition, 2013.
- [24] M. Iqbal, *An Introduction To Solar Radiation*, first edition, Elsevier, 1983.
- [25] T.A. Reddy, *Applied Data Analysis and Modeling for Energy Engineers and Scientists*, 2011.
- [26] F.J. Ms, *Hypothesis testing: an intuitive guide for making data driven decisions*, *J. Chem. Inf. Model.* (2019).
- [27] T.P. Chang, Investigation on frequency distribution of global radiation using different probability density functions, *Int. J. Appl. Sci. Eng.* (2010).
- [28] K. Emery, Uncertainty Analysis of Certified Photovoltaic Measurements at the National Renewable Energy Laboratory.
- [29] J.T. Nakos, Uncertainty analysis of thermocouple measurements used in normal and abnormal thermal environment experiments at Sandia's radiant heat facility and Lurance Canyon Burn Site, Sandia, 2004, [Online]. Available: <https://www.osti.gov/servlets/purl/918777>.
- [30] NREL, Solar Resource Glossary, [Online]. Available: <https://www.nrel.gov/grid/solar-resource/solar-glossary.html> [Accessed: 25-Aug-2022].
- [31] A.D. Matthias et al., Surface roughness effects on soil Albedo, *Soil Sci. Soc. Am. J.* (2000).
- [32] N. Sugathan, V. Biju, G. Renuka, Influence of soil moisture content on surface albedo and soil thermal parameters at a tropical station, *J. Earth Syst. Sci.* (2014).
- [33] C. Deline et al., Evaluation and field assessment of bifacial photovoltaic module power rating methodologies, in: IEEE 43rd Photovoltaic Specialists Conference, 2016.
- [34] Solar World, Calculating the Additional Energy Yield of Bifacial Solar Modules, 2015, [Online]. Available: <https://solaren-power.com/pdf/Calculating-Additional-Energy-Yield-Through-Bifacial-Solar-Technology.pdf>.
- [35] W. Porter, Bifacial Modules: There are two sides to every solar panel, 2021.
- [36] C. Tjengdrawira, M. Richter, T. Ioannis, Best Practice Guidelines for PV Cost Calculation, 2016.
- [37] E. and I.S. UK GOV, Department for Business, Quarterly Energy Prices, 2022.
- [38] M.L. Marceau, M.G. Vangeem, Solar Reflectance of Concretes for LEED Sustainable Sites Credit : Heat Island Effect, PCA R&D Ser. No. 2982, 2007.
- [39] The University of Tennessee Center for Clean Products, Case study: Natural Stone Solar Reflectance Index and the Urban Heat Island Effect, 2009.
- [40] A.L. Pisello, G. Pignatta, V.L. Castaldo, F. Cotana, Experimental analysis of natural gravel covering as cool roofing and cool pavement, *Sustain.* (2014).